

***In Vitro* and *In Silico* Analyses of Biomolecular Regulation of
Liposomal CRE-SD on Osteoclastogenesis via a
Canonical NF- κ B Signaling Pathway**

Sompot Jantarawong

**A Thesis Submitted in Partial Fulfillment of the Requirements for the Degree of
Master of Science in Molecular Biotechnology and Bioinformatics
(International program)**

Prince of Songkla University

2023

Copyright of Prince of Songkla University



***In Vitro* and *In Silico* Analyses of Biomolecular Regulation of
Liposomal CRE-SD on Osteoclastogenesis via a
Canonical NF- κ B Signaling Pathway**

Sompot Jantarawong

**A Thesis Submitted in Partial Fulfillment of the Requirements for the Degree of
Master of Science in Molecular Biotechnology and Bioinformatics
(International program)**

Prince of Songkla University

2023

Copyright of Prince of Songkla University

Thesis Title	<i>In Vitro</i> and <i>In Silico</i> Analyses of Biomolecular Regulation of Liposomal CRE-SD on Osteoclastogenesis via a Canonical NF- κ B Signaling Pathway
Author	Mr.Sompot Jantarawong
Major Program	Molecular Biotechnology and Bioinformatics

Major Advisor

.....
 (Asst. Prof. Dr. Yutthana Pengjam)

Examining Committee:

..... Chairperson
 (Assoc. Prof. Dr. Chairat Tantrawatpan)

Co-advisor

.....
 (Asst. Prof. Dr. Aekkaraj Nualla-ong)

..... Committee
 (Asst. Prof. Dr. Yutthana Pengjam)

..... Committee
 (Asst. Prof. Dr. Unitsa Sangket)

..... Committee
 (Asst. Prof. Dr. Aekkaraj Nualla-ong)

The Graduate School, Prince of Songkla University, has approved this thesis as partial fulfillment of the requirements for the Master of Science Degree in Molecular Biotechnology and Bioinformatics (International program).

.....
 (Asst. Prof. Dr. Thakerng Wongsirichot)

Acting Dean of Graduate School

This is to certify that the work here submitted is the result of the candidate's own investigations. Due acknowledgement has been made of any assistance received.

..... Signature

(Asst. Prof. Dr. Yutthana Pengjam)

Major Advisor

..... Signature

(Asst. Prof. Dr. Aekkaraj Nualla-ong)

Co-advisor

..... Signature

(Mr.Sompot Jantarawong)

Candidate

I hereby certify that this work has not been accepted in substance for any degree and is not being currently submitted in candidature for any degree.

..... Signature

(Mr.Sompot Jantarawong)

Candidate

ชื่อวิทยานิพนธ์	การวิเคราะห์กลไกการควบคุมทางชีวโมเลกุลของ liposomal CRE-SD ในกระบวนการสร้างเซลล์สลายกระดูกผ่านกลไกการส่งสัญญาณ canonical NF- κ B signaling pathway ด้วยวิธี <i>in vitro</i> และ <i>in silico</i>
ผู้เขียน	นายสมพจน์ จันทรวงศ์
สาขาวิชา	เทคโนโลยีชีวภาพโมเลกุลและชีวสารสนเทศ
ปีการศึกษา	2566

บทคัดย่อ

สารประกอบ curcuminoids ชนิด curcumin, demethoxycurcumin, และ bisdemethoxycurcumin เป็นสารสำคัญที่พบในขมิ้นชัน (*Curcuma longa* L.) แม้ว่าสารประกอบ curcuminoids ทั้งสามชนิดสามารถยับยั้งกระบวนการสลายกระดูก แต่สารประกอบ curcuminoids ยังคงมีสมบัติทางเภสัชจลนศาสตร์ที่ไม่เหมาะสม ด้วยเหตุนี้ ผู้วิจัยจึงพัฒนาสมบัติทางเภสัชจลนศาสตร์ของสารประกอบ curcuminoids โดยเตรียมสารสกัด curcuminoid-rich extract (CRE) ที่มีองค์ประกอบเป็นสาร curcuminoids ทั้งสามชนิด จากนั้น ผู้วิจัยใช้เทคนิค solid dispersion เพื่อเตรียมสาร CRE-SD จากสาร CRE ข้างต้น และห่อหุ้ม (encapsulate) CRE-SD ด้วย POPC liposomes จนเกิดเป็นสาร liposomal CRE-SD จากการทดลอง *in vitro* release ระบุว่า liposomal CRE-SD มีร้อยละของมวลสะสม (cumulative mass) ของ CRE-SD ที่ถูกปล่อยออกมาจาก dialysis sac น้อยกว่า liposomes ที่ไม่มีการห่อหุ้ม CRE-SD หลังจากเลี้ยงเซลล์ murine RAW 264.7 macrophages และกระตุ้นการสร้างเซลล์ osteoclasts โดยใช้ RANKL ผลการทดสอบ *in vitro* ยืนยันว่า liposomal CRE-SD สามารถยับยั้งการสร้างเซลล์สลายกระดูกผ่านการยับยั้งกลไก phosphorylation ของ p65 และ I κ B α รวมทั้งกลไก nuclear translocation และกลไกการถอดรหัส DNA (transcription) ของ p65 ที่มีการเติมหมู่ฟอสเฟต (phosphorylated p65) ผลการจำลองการจับกันระหว่างโมเลกุล (blind docking simulation) ระบุว่า สาร curcuminoids ทั้งสามชนิดมีความสามารถในการจับ (binding affinity) กับสารประกอบโปรตีนเชิงซ้อนของ I κ B α , p50 และ p65 รวมทั้งมีแรงยึดเหนี่ยวระหว่างโมเลกุล (intermolecular interactions) จำนวนมากต่อสารประกอบโปรตีนเชิงซ้อนดังกล่าว ซึ่งสอดคล้องกับผลการทดลอง *in vitro* ข้างต้น ดังนั้น liposomal CRE-SD จึงสามารถยับยั้งการสร้างเซลล์สลายกระดูกผ่านกลไกการส่งสัญญาณ canonical NF- κ B signaling

pathway ซึ่งอาจนำไปใช้ในการพัฒนาเป็นยารักษาโรคกระดูกที่มีการสร้างเซลล์สลายกระดูกมากกว่าปกติต่อไป

คำสำคัญ: curcuminoid; liposomal CRE-SD; การสร้างเซลล์สลายกระดูก; เซลล์ RAW 264.7 macrophage ที่ถูกกระตุ้นด้วย RANKL; canonical NF- κ B signaling pathway

Thesis Title	<i>In Vitro</i> and <i>In Silico</i> Analyses of Biomolecular Regulation of Liposomal CRE-SD on Osteoclastogenesis via a Canonical NF- κ B Signaling Pathway
Author	Mr.Sompot Jantarawong
Major Program	Molecular Biotechnology and Bioinformatics
Academic Year	2023

ABSTRACT

Curcuminoids, namely curcumin, demethoxycurcumin, and bisdemethoxycurcumin, are the major active compounds found in *Curcuma longa* L. (turmeric). Although their suppressive effects on bone resorption have been demonstrated, their pharmacokinetic disadvantages remain a concern. Herein, solid dispersion of a curcuminoid-rich extract (CRE), comprising such curcuminoids, was utilized to prepare CRE-SD; subsequently, liposome encapsulation of the CRE-SD was performed to yield liposomal CRE-SD. *In vitro* release assessment revealed that a lower cumulative mass percentage of CRE-SD was released from liposomal CRE-SD than from CRE-SD samples. After culture of murine RANKL-stimulated RAW 264.7 macrophages, *in vitro* examinations confirmed that liposomal CRE-SD may impede osteoclastogenesis by suppressing p65 and I κ B α phosphorylation, together with nuclear translocation and transcriptional activity of phosphorylated p65. Blind docking simulations showed the high binding affinity between curcuminoids and the I κ B α /p50/p65 protein complex, along with many intermolecular interactions, which corroborated the *in vitro* findings. Therefore, liposomal CRE-SD can inhibit osteoclastogenesis via the canonical NF- κ B signaling pathway, suggesting its pharmacological potential for treating bone diseases with excessive osteoclastogenesis.

Keywords: curcuminoid; liposomal CRE-SD; osteoclastogenesis; RANKL-stimulated RAW 264.7 macrophage; canonical NF- κ B signaling pathway

ACKNOWLEDGEMENT

First, I would like to express my sincere gratitude to Asst. Prof. Dr. Yutthana Pengjam (major advisor and thesis examination committee) and Asst. Prof. Dr. Aekkaraj Nualla-ong (co-advisor and thesis examination committee) for outstanding supervision, academic consultation, and emotional support. I am also deeply grateful to Assoc. Prof. Dr. Chairat Tantrawatpan (thesis examination chairperson) and Asst. Prof. Dr. Unitsa Sangket (thesis examination committee) for suggesting constructive feedback during thesis proofreading and thesis defense examination.

In terms of financial funding, I would like to acknowledge the Faculty of Medical Technology Research Fund, Prince of Songkla University for providing me with an opportunity to study for the Master of Science in Molecular Biotechnology and Bioinformatics. Additionally, this thesis cannot be successful without financial granting from the Thesis Research Grant in the Fiscal Year 2022, Graduate School, Prince of Songkla University.

I am extremely thankful to Enago for suggesting magnificent and thorough comments in the English editing. Regardless of this help, the research publication fulfilling the M.Sc. graduation would not be complete.

I would like to give many thanks to all the lecturers as well as all the fellow Ph.D. and M.Sc. students for sharing their expertise and giving encouragement. I am also grateful to all the staff of the Faculty of Science, Prince of Songkla University for advising me throughout my thesis progression.

Lastly, I would like to thank my family, along with all the teachers and friends in my childhood and my B.Sc. life, for believing in my determination and staying beside me.

Sompot Jantarawong

CONTENT

	Page
บทคัดย่อภาษาไทย (THAI ABSTRACT)	v
ENGLISH ABSTRACT	vii
ACKNOWLEDGEMENT	viii
CONTENT	ix
LIST OF TABLES	xii
LIST OF FIGURES	xiii
LIST OF ABBREVIATIONS AND SYMBOLS	xv
CHAPTER 1 INTRODUCTION	1
1.1 Background and Rationale	1
1.2 Review of Literature	4
1.2.1 Bone homeostasis	5
1.2.2 Synthetic drugs for treating bone diseases with abnormal bone homeostasis	6
1.2.3 Turmeric and curcuminoids	9
1.2.4 Improving pharmacokinetic properties of curcuminoids	9
1.2.5 NF- κ B signaling pathway	11
1.2.6 Molecular docking simulation	15
1.2.7 Discussion	16
1.3 Objectives	17
CHAPTER 2 RESEARCH METHODOLOGY	18
2.1 <i>In vitro</i> experiments	18
2.1.1 Cells and reagents	18
2.1.2 Preparation, characterization, and <i>in vitro</i> release of liposomal CRE-SD	18
2.1.3 Culture of RAW 264.7 cells	19
2.1.4 Evaluation of optimal RANKL incubation time in RAW 264.7 cells treated with CRE-SD-free POPC liposomes (CRE-SD-FREE-LIP)	19
2.1.5 Viability examination of liposomal CRE-SD-treated RAW 264.7 cells	20

CONTENT (continued)

	Page
2.1.6 Confirmation of osteoclastogenic inhibition in liposomal CRE-SD-treated RANKL-stimulated RAW 264.7 cells	20
2.1.7 Primer sequences for RT-PCR and qRT-PCR amplification	21
2.1.8 Detection of phosphorylation of p65 and I κ B α proteins in liposomal CRE-SD-treated RANKL-stimulated RAW 264.7 cells	22
2.1.9 Confirmation of the inhibitory effect of liposomal CRE-SD on nuclear translocation and transcriptional activity of phosphorylated p65 (p-p65)	22
2.1.10 Detecting intracellular ROS production	22
2.1.11 Statistical analysis	23
2.2 <i>In silico</i> analyses	23
2.2.1 Retrieval of the structures of the I κ B α /p50/p65 complex and curcuminoids	23
2.2.2 Blind docking simulation between the I κ B α /p50/p65 complex and Cu/De/Bis	23
CHAPTER 3 RESULTS	25
3.1 Liposomal CRE-SD characterization	25
3.2 <i>In vitro</i> assessment of CRE-SD release	25
3.3 Optimization of RANKL incubation time	26
3.4 Optimization of liposomal CRE-SD concentration	26
3.5 Inhibitory effect of liposomal CRE-SD on osteoclastogenesis	27
3.6 Suppressive effect of liposomal CRE-SD on I κ B α /p65 phosphorylation in osteoclastogenesis	28
3.7 Inhibitory effect of liposomal CRE-SD on nuclear translocation and transcriptional activity of p-p65 in osteoclastogenesis	30
3.8 Inhibition of liposomal CRE-SD on intracellular ROS production in osteoclastogenesis	31
3.9 Blind docking simulation between I κ B α /p50/p65 protein complex and Cu/De/Bis	32
3.10 The Inhibitory Effect of Liposomal CRE-SD on Osteoclastogenesis via the Canonical NF- κ B Signaling Pathway	38
CHAPTER 4 DISCUSSION	39
CHAPTER 5 CONCLUSION	46

CONTENT (continued)

	Page
BIBLIOGRAPHY	47
APPENDIX	56
Appendix A: The triplicate data of microscopic images, gel images, and blot images	57
VITAE	62

LIST OF TABLES

	Page
Table 1 Examples of current anti-osteoporosis drugs	6
Table 2 Solid dispersion and liposome/nanoliposome encapsulation	10
Table 3 Comparison between canonical and noncanonical NF- κ B signaling pathways	12
Table 4 Liposomal characteristics	25
Table 5 CurPocket-based information on the five largest binding pockets of I κ B α /p50/p65 protein complex	33
Table 6 Possible contact residues of five predicted binding pockets of I κ B α /p50/p65 protein complex derived from CurPocket	34
Table 7 The I κ B α /p50/p65 binding pockets with the greatest negative Vina scores after blind docking with curcuminoids	35
Table 8 Possible contact residues of the I κ B α /p50/p65 binding pockets in Table 7	36

LIST OF FIGURES

	Page
Figure 1 Three-dimensional chemical structures	3
Figure 2 Liposomal CRE-SD preparation process	4
Figure 3 Various cells involved in the bone homeostasis	5
Figure 4 Canonical NF- κ B signaling pathway	13
Figure 5 Noncanonical NF- κ B signaling pathway	14
Figure 6 <i>In vitro</i> assessment of CRE-SD release after liposomal encapsulation	26
Figure 7 Optimization of RANKL incubation time and liposomal CRE-SD concentration	27
Figure 8 Osteoclastogenic examination	29
Figure 9 Regulatory effect of liposomal CRE-SD on p65 and I κ B α phosphorylation	30
Figure 10 Regulatory effect of liposomal CRE-SD on p65 phosphorylation after incorporating JSH23	31
Figure 11 Percentage of intracellular reactive oxygen species (ROSs) produced in 20 ng/mL RANKL-stimulated RAW 264.7 cells	32
Figure 12 The 3D structures of five predicted binding pockets of I κ B α /p50/p65 protein complex derived from CurPocket	33
Figure 13 CB-Dock2 blind docking results of the I κ B α /p50/p65 protein complex and curcumin/demethoxycurcumin/bisdemethoxycurcumin	37
Figure 14 The inhibitory effect of liposomal CRE-SD on osteoclastogenesis via the canonical NF- κ B signaling pathway	38
Figure A1 Triplicate microscopy images of 20 ng/mL RANKL-stimulated RAW 264.7 cells (osteoclasts) after TRAP staining following treatment with CRE-SD-free POPC liposomes (CRE-SD-FREE-LIP) and 20 μ g/mL liposomal CRE-SD	57

LIST OF FIGURES (continued)

	Page
Figure A2 Triplicate microscopy images of 20 ng/mL RANKL-stimulated RAW 264.7 cells (osteoclasts) after the immunocytochemistry analysis of F4/80	58
Figure A3 Triplicate images of gels analyzing 20 ng/mL RANKL-stimulated RAW 264.7 cells (osteoclasts) following RT-PCR analysis of CTSK, c-Fos, and NFATc1	59
Figure A4 Triplicate images of blots analyzing 20 ng/mL RANKL-stimulated RAW 264.7 cells (osteoclasts) following the detection of the phosphorylation of p65 and I κ B α	60
Figure A5 Triplicate images of blots of 20 ng/mL RANKL-stimulated RAW 264.7 cells (osteoclasts) for detecting the nuclear translocation and transcriptional activity of p-p65	61

LIST OF ABBREVIATIONS AND SYMBOLS

Å: angstrom

AnkRs: ankyrin repeats

BAFF-Rs: B-cell activating factor receptors

Bis: bisdemethoxycurcumin

BSA: bovine serum albumin

CADD: computer-aided drug design

CASTp: Computed Atlas of Surface Topography of Proteins

CID: compound identifier

CTSK: cathepsin K

CRE: curcuminoid-rich extract

CRE-SD: curcuminoid-rich extract with PVP K30 solid dispersion

CRE-SD-FREE-LIP: CRE-SD-free POPC liposomes

CRE-Ter: CRE ternary complex modified with PVP K30 and HPBCD

Cu: curcumin

DAB: 3,3'-diaminobenzidine

DCF: 2',7'-dichlorofluorescein

De: demethoxycurcumin

DLS: dynamic light scattering

DMPC: 1,2-dimyristoyl-*sn*-glycero-3-phosphocholine

DOPC: 1,2-dioleoyl-*sn*-glycero-3-phosphocholine

ERK: extracellular signal-regulated kinase

FBS: fetal bovine serum

GRAS: Generally Recognized As Safe

HPBCD: 2-hydroxypropyl- β -cyclodextrin

HPMCE5: hydroxypropyl methyl cellulose

HRP: horseradish peroxidase

HSC: hematopoietic stem cell

LIST OF ABBREVIATIONS AND SYMBOLS (continued)

I κ B α : I κ B inhibitor α

IKK: I κ B kinase

IL-6: interleukin-6

IL-17: interleukin-17

IL-1RI: interleukin 1 receptors, type I

JSH23: (4-methyl-N1-(3-phenylpropyl)-1,2-benzenediamine

LT β Rs: lymphotoxin β receptors

MAC: complement membrane attack complex

NEMO: NF- κ B essential modifier

NFATc1: nuclear factors of activated T cells 1

NF- κ B: nuclear factor kappa light chain enhancer of activated B cells

NIK: NF- κ B-inducing kinase

NLS: nuclear localization sequence

PBS: phosphate-buffered saline

PDB: Protein Data Bank

PDI: polydispersity index

PEG: polyethylene glycol

p-I κ B α : phosphorylated I κ B α

POPC: 1-palmitoyl-2-oleoyl-phosphatidylcholine

p-p65: phosphorylated p65

PVP K30: polyvinylpyrrolidone K30

RA: rheumatoid arthritis

RANK: receptor activator of nuclear factor- κ B

RANKL: receptor activator of nuclear factor- κ B ligand

RHR/RHD: Rel homology region/Rel homology domain

RMSD: root mean squared deviation

ROS: reactive oxygen species

LIST OF ABBREVIATIONS AND SYMBOLS (continued)

SEM: scanning electron microscope

SPC: soybean phosphatidylcholine

TAD: transactivation domain

TCP: tricalcium phosphate

TCRs: T-cell receptors

TEM: transmission electron microscope

TLRs: toll-like receptors

TNF: tumor necrosis factor

TNF- α : tumor necrosis factor- α

TPGS: D- α -tocopherol polyethylene glycol 1000 succinate

TRAP: tartrate-resistant acid phosphatase

CHAPTER 1

INTRODUCTION

1.1 Background and Rationale

Bone homeostasis dynamically regulates the coupling of bone formation and bone resorption. Osteoclasts are large bone breakdown cells that function in collaboration with osteoblasts (bone-forming cells), osteocytes, and other cells in the bone homeostasis mechanism. Osteoclastogenesis (osteoclast differentiation) can be stimulated by the specific binding between the receptor activator of nuclear factor- κ B ligand (RANKL) and the receptor activator of nuclear factor- κ B (RANK) of the RAW 264.7 macrophages—the osteoclast precursors [1–3]. After osteoclastogenesis is complete, multinucleated microscopic appearance can be detected, as well as an increased expression of osteoclast markers (e.g., cathepsin K (CTSK), tartrate-resistant acid phosphatase (TRAP), c-Fos, and the nuclear factors of activated T cells 1 (NFATc1) [4,5]. Many previous reports have revealed that the immoderate osteoclast activity, surpassing bone resorption, leads to an imbalance in bone homeostasis and, subsequently, results in some types of bone diseases, such as osteoporosis and rheumatoid arthritis (RA) [6,7]. This has contributed to the design of drugs impeding the excessive osteoclast action that occurs during the treatment of bone diseases. To achieve this, experimental (*in vitro* and *in vivo*) and computational or bioinformatics (*in silico*) analyses that elucidate the biochemical effects of drugs on osteoclasts are required. The inhibitory effects of various anti-osteoporotic and antirheumatic synthetic drugs on osteoclast activities have been explained [8,9]. Furthermore, an *in silico* experimental method known as molecular docking was used to demonstrate that some established drugs, such as CTSK inhibitors and interleukin 6 inhibitors, can interact with protein targets to hamper osteoclast differentiation and alleviate bone diseases [10,11]. Despite the benefits in pharmaceutical practice, the serious side effects of synthetic drugs for the treatment of osteoporosis and RA are of concern [10,12]. Hence, advances in herbal extracts and an examination of the molecular roles of herbal extracts are alternative approaches that may lead to effective treatments for bone diseases.

Curcuma longa L. (turmeric) is a rhizomatous perennial in the Zingiberaceae (ginger) family planted in tropical and subtropical regions worldwide. It is widely utilized as an herbal medicine, owing to its manifold pharmacological properties, including antibacterial, anticancer, antioxidant, anti-inflammatory, and antiproliferative effects [13–15]. Curcuminoids—the main active ingredients in turmeric—are phenolic compounds commonly extracted for the aforementioned medicinal uses. The US Food and Drug Administration has classified these compounds as “Generally Recognized as Safe” (GRAS) [13,14]. The curcuminoid termed curcumin (Cu) is present in the highest proportion (approximately 80%), followed by demethoxycurcumin (De), and then by bisdemethoxycurcumin (Bis) [15,16]. The three-dimensional (3D) chemical structures of each curcuminoid are illustrated in Figure 1A–

C. Numerous *in vitro* and *in vivo* studies, together with clinical trials, have shown that each of these curcuminoids can inhibit bone resorption and may be promising remedies for bone diseases [17–19]. Huang et al. [20] demonstrated the synergistic effects of typical treatment for HOS cancer cells *in vitro* with a combination of Cu, De, and Bis, compared with a combination containing only one or two of the curcuminoids. This finding suggests the prospect of employing such an herbal combination for osteosarcoma therapy. Although these biomedical examinations have corroborated the potential of curcuminoids in the management of bone diseases, curcumin pharmacokinetics are not ideal, as there are still many issues to consider, namely: restricted bioavailability, limited absorption in the small intestine, fast metabolism, and fast systemic elimination. Additionally, curcumin is hydrophobic and has low solubility in water, as it contains *o*-methoxy and phenolic groups [14,21,22]. In an effort to address these issues, various techniques through which to improve the pharmacokinetic attributes of curcumin have been applied; examples include preparing curcumin as a solid dispersion (dispersing the hydrophobic molecule in an inert carrier such as a synthetic polymer) and using liposomal encapsulation [22]. The superior water solubility and absorption properties of solid dispersion-based curcumin and liposomal curcumin compared with pure curcumin have been revealed in some recent studies [23,24]. However, these pharmacological attributes have not yet been proven for the combination of Cu, De, and Bis modified by integrating both abovementioned formulation techniques. Moreover, the biomolecular regulatory effects of these newly developed forms of curcuminoids on osteoclast differentiation and bone resorption are yet to be elucidated.

The downstream signaling pathways of the nuclear factor kappa-light-chain-enhancer of activated B cells (NF- κ B) are crucial for osteoclastogenic stimulation. In the canonical (classical) NF- κ B signaling pathway, p50 (originating from the proteolysis of the p105 precursor protein) and p65 (Rel A) serve as transcription factors. When RANKL interacts with RANK on the surface of osteoclast precursors (in a mechanism called the RANKL–RANK upstream signaling pathway), the cytoplasmic adaptor molecules in the canonical NF- κ B signaling pathway are subsequently activated. Then, the cytoplasmic inhibitor of the I κ B kinase (IKK) complex, comprising two catalytic kinase subunits (IKK α and IKK β) and at least one noncatalytic regulatory subunit known as the NF- κ B essential modifier (NEMO), or IKK γ , regulates the phosphorylation of a specific subunit in the I κ B inhibitor α (I κ B α)/p50/p65 protein complex. The 3D structure of the I κ B α /p50/p65 complex is shown in Figure 1D. Activated IKK β phosphorylates I κ B α , whereas IKK α phosphorylates p65. Afterward, the phosphorylated I κ B α (p-I κ B α) is polyubiquitinated and degraded by the 26S proteasome, whereas the p50/p65 heterodimer—the most structurally stable form of the NF- κ B dimer—freely translocates to the nucleus to transcribe its target genes [25–30]. Previous *in vitro* experiments revealed that curcumin can hinder the phosphorylation and degradation of I κ B α , as well as the nuclear translocation of p65 [31]. By applying curcumin as a cell treatment, the phosphorylation of I κ B α and p65 in osteoclasts, namely RANKL-stimulated RAW

264.7 macrophages, was suppressed, which eventually suppressed osteoclastogenesis [32,33]. In molecular docking simulations, Cheemanapalli et al. used AutoDock version 4.0 to show that there were binding interactions between curcumin and the specific active site residues of each major protein in the canonical NF- κ B pathway, especially the IKK complex, proteasome, and p65 [34]. In addition, Saeed et al. demonstrated strong binding affinity between the I κ B α /p50/p65 complex and diverse curcumin compounds (including Cu, De, Bis, etc.) using AutoDock version 4.2.6 [35].

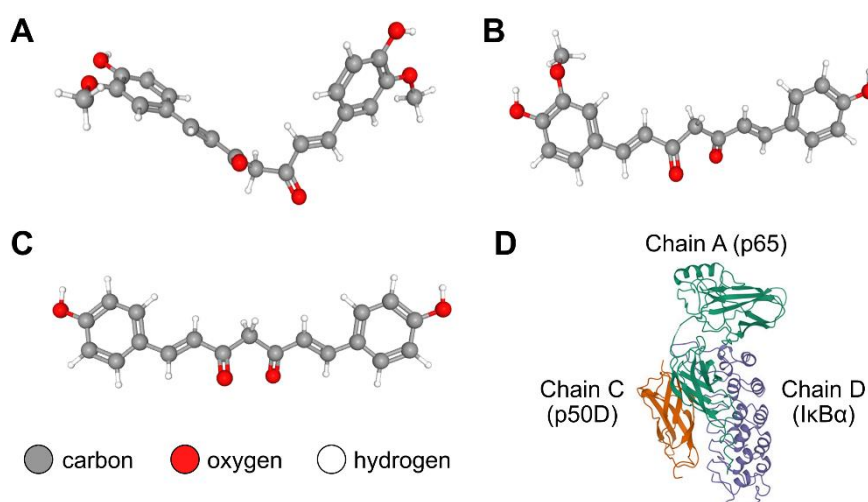


Figure 1 Three-dimensional chemical structures

Three-dimensional chemical structures of (A) curcumin (Cu; PubChem compound identifier (CID): 969516); (B) demethoxycurcumin (De; PubChem CID: 5469424); (C) bisdemethoxycurcumin (Bis; PubChem CID: 5315472); and (D) I κ B α /p50/p65 protein complex (Protein Data Bank (PDB) ID: 1IKN, consisting of p65 (chain A), p50D (chain C), and I κ B α (chain D) subunits). The structures of the curcuminoid substances (Cu, De, and Bis) and the protein complex were retrieved from the PubChem and PDB databases, respectively.

Although several *in vitro* and bioinformatics investigations have evidenced the protective effect of curcumin on the canonical NF- κ B pathway in osteoclast differentiation, the biomolecular mechanism has not been fully explained for the combination of Cu, De, and Bis modified by utilizing both solid dispersion and liposomal encapsulation techniques. To fill these knowledge gaps, a curcuminoid-rich extract (CRE), containing Cu, De, and Bis, was prepared from the dried powders of *C. longa* rhizomes, and employed the synthetic polymer polyvinylpyrrolidone K30 (PVP K30) to produce a solid dispersion, as illustrated in Figure 2. After obtaining the CRE with PVP K30 solid dispersion (CRE-SD) from this process, it was encapsulated in liposomes to derive liposomal CRE-SD. Subsequently, the characteristics of the liposomal CRE-SD were evaluated and an *in vitro* analysis of its biomolecular involvement in the canonical NF- κ B pathway of murine RANKL-stimulated RAW

264.7 macrophages was performed. Moreover, to illustrate the molecular interactions, a blind docking simulation between the $\text{I}\kappa\text{B}\alpha/\text{p}50/\text{p}65$ complex and each of the curcuminoids, was implemented using the web-based molecular docking tool CB-Dock2.

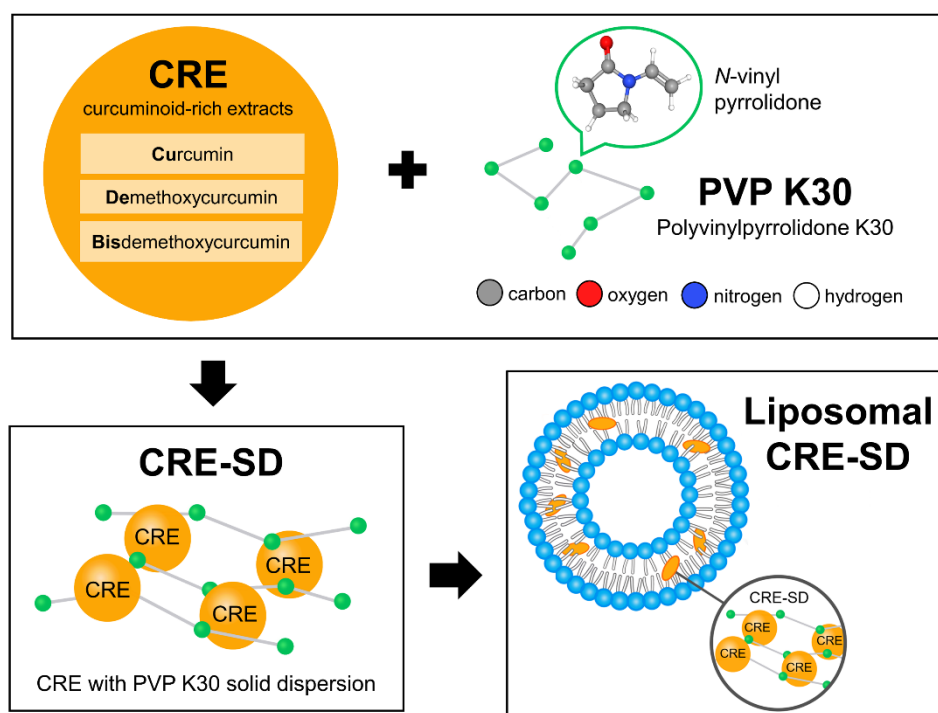


Figure 2 Liposomal CRE-SD preparation process

The dried powders of *Curcuma longa* rhizomes were applied to derive a curcuminoid-rich extract (CRE) comprising curcumin, demethoxycurcumin, and bisdemethoxycurcumin. To obtain CRE-SD with 7% *w/w* of curcuminoids, the resulting CRE was modified with polyvinylpyrrolidone K30 (PVP K30)—the synthetic polymer produced from the monomer termed *N*-vinyl pyrrolidone—using the solid dispersion technique. To obtain liposomal CRE-SD, the liposomal encapsulation method was subsequently used to interpose the CRE-SD in the lipid bilayer of the POPC liposomes.

1.2 Review of Literature

Nowadays, the advance of drugs of bone diseases with excessive bone resorption has been accumulated, especially herbal extract. In this study, the liposomal CRE-SD – the modified form of CRE – was prepared to assess its pharmacokinetic properties, osteoclastogenic suppression *in vitro*, and molecular interactions to the $\text{I}\kappa\text{B}\alpha/\text{p}50/\text{p}65$ protein complex, implying its pharmaceutical performance in alleviating such bone diseases. To elucidate the related theories from previous research, the content in this section - the literature review - is split into 7 subsections: bone homeostasis,

synthetic drugs for treating bone diseases with abnormal bone homeostasis, turmeric and curcuminoids, improving pharmacokinetic properties of curcuminoids, NF- κ B signaling pathway, molecular docking simulation, and discussion. Here, the scope of the literature review is limited to the mechanisms in cellular and biomolecular levels, while the mechanisms in systemic and organ-specific levels are not mainly focused.

1.2.1 Bone homeostasis

Physiological homeostasis is the dynamic mechanism that maintains internal equilibrium in diverse organisms, notably mammals [36,37]. The mammalian bones – the organ-supporting components – has a major significance in bone development and bone repair. Previous reports found the imbalance of bone homeostasis in bone diseases, e.g., osteoporosis [38], osteoarthritis with bone cell dysfunction [39], RA stimulated by bone degradation [40], etc. In addition, bone remodeling – the end-stage of bone repair – is modulated by the bone homeostasis. Accordingly, many researchers have endeavored to analyze the cellular and biomolecular mechanisms affecting bone homeostasis of bone diseases to develop the therapeutic approaches.

There are many crucial cells involved in bone homeostasis (Figure 3), consist of osteoblasts (bone-forming cells), osteoclasts (bone-breakdown cells), osteocytes, etc. [2,41,42]. Osteoblasts – differentiated from preosteoblasts – regulate skeletal strengthening via bone mineralization and osteocyte differentiation. Osteoclasts – differentiated from monocyte/macrophage lineage – are large multinucleated cells playing a major role in bone mass control and bone remodeling [4]. To stimulate the osteoclast differentiation, the RANKLs are secreted from the osteocytes and specifically bind to the RANK receptors of osteoclast precursors, e.g., RAW 264.7 macrophages [1-3]. After the differentiation process is complete, the multinucleated morphology can be microscopically observed; moreover, the osteoclast markers (TRAP, CTSK, c-Fos, and NFATc1) are highly expressed [4,5].

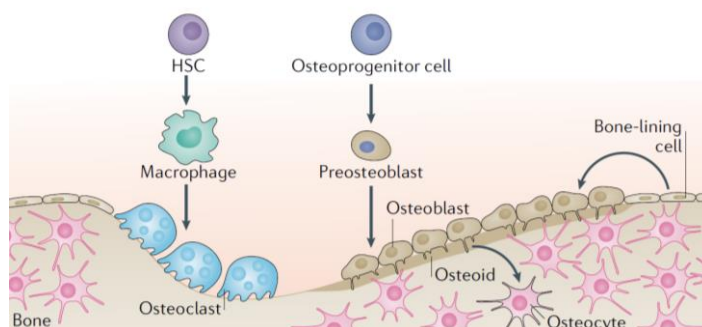


Figure 3 Various cells involved in the bone homeostasis

The figure is referred from [2]. HSC: hematopoietic stem cell.

Since some studies revealed that disrupting of bone homeostasis, which brings about immoderate osteoclast activity and high bone resorption, can contribute to the aforementioned bone diseases [6,7], manifold drugs have been designed for the treatment. These medicines will be exemplified in the next subsection.

1.2.2 Synthetic drugs for treating bone diseases with abnormal bone homeostasis

Osteoporosis

Osteoporosis – a bone disease with high bone fragility, low bone density and mass, and a susceptibility to bone fracture – can be mainly attributed to bone metabolic disorder as well as osteoblast inactivation resulting in diminished bone tissue and upregulated bone resorption [43]. At present, the drugs for osteoporotic treatment can be classified into 4 groups: antiresorptive agents, anabolic agents, drugs with other mechanisms of action, and targeted anti-osteoporosis agents [9]. The examples of the anti-osteoporosis drugs are illustrated in Table 1.

Table 1 Examples of current anti-osteoporosis drugs

Types	Drugs	Administration Pathways	Mechanism of action
antiresorptive agents			
bisphosphonates	Alendronate	oral administration	induce osteoclast apoptosis, inhibit osteoclast recruitment on the bone surface, induce osteoclast apoptosis
	zoledronic acid	oral administration	
	Risedronate	oral administration	
	ibandronate	oral administration	
	etidronate disodium	oral administration	
	clodronate disodium	oral administration	
hormone replacement therapy	estrogen/progestogen	oral administration	inhibit RANKL/RANK activation, inhibit oxidative stress, inhibit local inflammation
	raloxifene	oral administration	
Calcitonin	elcatonin	intramuscular injection	inhibit osteoclast activity, inhibit acid hydrolase release, reduce osteoclast adhesion on bone surface, reduce blood calcium concentration
	salmon calcitonin	intramuscular injection, inhalation	

Types	Drugs	Administration Pathways	Mechanism of action
anabolic agents			
parathyroid hormone and its analogs	abaloptide	inhalation	regulate serum calcium and phosphorus ion concentration
	teriparatide	inhalation	
Fluoride	NA	NA	promote osteoblast proliferation and activation by 1) stimulating the differentiation of mesenchymal stem cells into osteoblasts 2) suppressing acid phosphatase activity in osteoblasts
growth hormone	NA	NA	activate osteoblasts and stimulate bone remodeling
Statins	NA	NA	unclear
drugs with other mechanisms of action			
vitamin D and its analogs	α -calciferol	oral administration	regulate calcium and phosphorus reabsorption
	Calcitriol	oral administration	
Strontium	strontium ranelate	oral administration	regulate Runx2, activate non-classical Wnt pathway, inhibit RANKL/RANK-induced osteoclast differentiation
vitamin K	Menatetrenone	oral administration	enhance cartilage protection
targeted anti-osteoporosis agents			
targeted anti-osteoporosis agents	Denosumab (RANKL inhibitor in monoclonal antibody form)	inhalation	specific targeting to RANKL
	Odanacatib (CTSK inhibitor)	oral administration	selective inhibitor of CTSK

NOTE: This table is referred from [9]. NA: not applicable

Osteoarthritis

Osteoarthritis is a non-inflammatory degenerative joint disorder which the articular cartilage and other joint tissues are irreversibly destructed. It can be caused by interfering the bone cell mechanism and some anti-osteoarthritis drugs may interact to molecules involving in such mechanism [44]. MIV-711 – a CTSK inhibitor – can lessen joint pathology in osteoarthritic rabbits and decelerate degeneration of bone and cartilage in patients with primary knee osteoarthritis. Despite the absence of the finding, the anti-osteoarthritis effect of denosumab interacting to RANKL for osteoclastogenic inhibition was tested in erosive and knee osteoarthritis [44]. Nevertheless, there are no anti-osteoarthritis drugs which have disease-modifying property (the capability to prevent the underlying pathophysiology directly) [44,45].

Rheumatoid arthritis

RA is a chronic inflammatory disease with an inflammation of synovial tissues in multiple small joints, together with dysregulation of bone formation–bone resorption coupling. Some proinflammatory cytokines, e.g., tumor necrosis factor- α (TNF- α), interleukin-6 (IL-6), interleukin-17 (IL-17), etc. can induce an increase in the RANKL expression during the disease progression, leading to an abnormality of bone homeostasis as well as bone erosion [8,46]. Many synthetic drugs have been utilized for RA treatment. Mrid et al. review mentioned that tofacitinib can interact to RANKL for RANKL downregulation, inhibiting excessive bone resorption, and alleviating joint damage. Hydroxyapatite can stimulate osteoblast adhesion to relieve joint damage [46]. Hauser et al. review referred the inhibitory effect of denosumab on osteoclast differentiation and activity. This drug may accordingly hamper the progression of joint erosion [8]. Furthermore, both Hauser et al. and Mrid et al. reviews suggested the anti-rheumatoid attributes of various inhibitors binding to the preceding proinflammatory cytokines. The interactions between the cytokines and the inhibitors may decrease the RANKL production and ameliorate the unbalanced bone formation–bone resorption coupling [8,46].

Side effects

Although the synthetic drugs previously exemplified can treat the bone diseases by modulating the bone mechanism, they have some side effects. For example, gastrointestinal problems from the administration of oral bisphosphonate; myocardial infarction, stroke, pulmonary emboli, and deep vein thrombosis from administrating conjugated equine estrogen in breast cancer women; transient orthostatic hypotension, leg cramps, and nausea from medicating teriparatide (a synthetic fragment of human parathyroid hormone); deep vein thrombosis from taking raloxifene; hypersensitivity reactions from treating with denosumab [12], etc. To address these, other therapeutic approaches for bone diseases have been developed, particularly herbal remedy. In the

next subsection, the pharmacological studies of using medicinal plant named turmeric for bone disease treatment will be explained.

1.2.3 Turmeric and curcuminoids

Turmeric (*Curcuma longa* L.) – a rhizomatous perennial in *Zingiberaceae* (ginger) family – found in tropical and subtropical regions worldwide. It has various pharmacological properties, e.g., antibacterial, anticancer, antioxidant, anti-inflammatory, and antiproliferative effects [13-15]. The turmeric contains the phenolic compounds that are the main active ingredient called curcuminoids (including Cu (approximately 80%), De, and Bis). They have been classified as “Generally Recognized as Safe” (GRAS) by the US Food and Drug Administration [13,14]. Sivani et al. review elucidated the therapeutic benefits of curcumin in RA patients by downregulating proinflammatory cytokines, along with inhibiting osteoclastogenesis and bone resorption [19]. Inchingolo et al. demonstrated that Cu may stimulate osteoblast activity, hinder osteoclast activity stimulated by RANKL-RANK interaction, and consequently improve bone density for osteoporotic alleviation. These biological mechanisms were corroborated by *in vitro* and *in vivo* analyses as well as clinical trial [47]. Shen et al. research showed the regulation of De to block osteoclast differentiation through JNK and extracellular signal-regulated kinase (ERK) signaling pathways (confirmed by *in vitro* experiments) and suppressing bone destruction attributed to tumor bone metastasis (proven by *in vivo* experiments) [17]. Wei et al. explored the stimulating effect of Bis on the differentiation of human amniotic mesenchymal stem cells into osteoblasts. Furthermore, subjecting the combination of Bis and the stem cells contributed to the synergistic amelioration on bone homeostasis in ovariectomy-induced osteoporosis mouse model [18]. In addition to incorporating each curcuminoid individually, Huang et al. found that a combination of Cu, De, and Bis synergistically activated the apoptosis of HOS cells, in comparison with one or two of the curcuminoids. Such herbal combination inferred its feasibility to treat primary malignant bone tumor called osteosarcoma [20]. Hence, Cu, De, and Bis can be safe and effective herbal compounds for the improvement of bone formation–bone resorption coupling and bone diseases. However, the curcumin has pharmacokinetic downsides, i.e., it has low bioavailability and is poorly absorbed in the small intestine, rapidly metabolized, and fast eliminated after the oral administration in human body [14,21,22]. The possible explanation is the hydrophobicity and low water solubility of the curcumin because of *o*-methoxy and phenolic groups in its chemical structure [21,22]. Therefore, diverse strategies have been applied to improve such curcuminoid pharmacokinetic properties, which will be illustrated in the next subsection.

1.2.4 Improving pharmacokinetic properties of curcuminoids

Sabet et al., Tabanelli et al., and Racz et al. reviews provided examples of the techniques for ameliorating the curcumin pharmacokinetic properties [22,48,49].

Here, the techniques called solid dispersion and liposome/nanoliposome encapsulation will be focused. Their general information is shown in Table 2.

Table 2 Solid dispersion and liposome/nanoliposome encapsulation

Strategy and description	Principle and fabrication
<p>Solid dispersion: It can be classified into 3 types upon the inert carrier utilized.</p> <ol style="list-style-type: none"> 1. first-generation crystalline solid dispersion: use crystalline carriers, e.g., urea, sucrose, dextrose, or galactose. 2. second-generation solid dispersion: use non-crystalline solid carrier or amorphous polymer. The carrier can be synthetic polymer or natural product-based polymer. 3. third-generation solid dispersion: use surfactant or a mixture of amorphous polymers and surfactants. 	<p>The hydrophobic molecules are dispersed in an inert carrier which has water solubility in solid state. There are 3 methods of solid dispersion.</p> <ol style="list-style-type: none"> 1. melting method: dissolving hydrophobic molecules in a liquid and adding the melted polyethylene glycol (PEG) to the resulting solution, without evaporation of the solvent. 2. melt agglomeration method: adding the molten carrier containing the hydrophobic molecules to the heated excipients. 3. solvent evaporation method: dissolving the hydrophobic molecules and carrier in a volatile solvent and subsequently evaporating the hydrophobic molecules.
<p>Liposome and nanoliposome encapsulation: Liposomes are self-assembled spherical particles that their aqueous core is enclosed by amphiphilic phospholipid bilayer (s), i.e., having outward hydrophilic heads and inward hydrophobic tails. The liposomes that have lower than 100 nm of diameter are named nanoliposomes. Because liposomes and nanoliposomes can transport the hydrophobic drugs via facilitated diffusion or pinocytosis across lipophilic cell membranes, they are highly biocompatible and have high affinity in biological system.</p>	<ol style="list-style-type: none"> 1. Incorporating organic solvents to the hydrophobic molecules. 2. pH-driven procedure: deprotonating and dissolving the hydrophobic molecules under alkaline conditions, and subsequently neutralizing them with an acidic solution of surfactants. After mixing the solutions, which decreases the pH, the hydrophobic molecules will precipitate and segregate inside the surfactant molecules. All the process is free from organic solvents.

NOTE: The information in the table is referred from [22,48,49].

Many recent studies have substantiated the improvement in pharmacokinetic properties of curcuminoids after implementing solid dispersion and liposome/nanoliposome encapsulation. Song et al. proved that employing solid dispersion with a lipid named krill oil and a stabilizer called aminoclay to curcumin led

to greater than 90% of drug dissolution within an hour, as opposed to pure curcumin. Moreover, the solid dispersion-modified curcumin had better absorption after oral administration in rats [23]. Ishtiaq et al. used kneading as well as solvent evaporation methods and incorporated PEG 6000, hydroxypropyl methyl cellulose (HPMCE5), PVP K30, and bovine serum albumin (BSA) to curcumin to prepare the solid dispersion. Their findings confirmed superior solubility and *in vitro* dissolution of HPMCE5- and PVP K30-solid dispersion-modified curcumin, in contrast to pure curcumin [50]. Mai et al. prepared the curcumin solid dispersion with 2-hydroxypropyl- β -cyclodextrin (HPBCD) by using grinding, freeze-drying, and solvent evaporation methods. These strategies increased the solubility and dissolution efficiency of curcumin [51]. Considering liposome/nanoliposome encapsulation, the study of Sinjari et al. showed more negative value of zeta potential after the curcumin was encapsulated to POPC liposomes, indicating higher stability of the curcumin [52]. The *in vitro* release profile in Sarkar and Bose research showed 17% and 30.9% of the curcumin cumulative release in DMPC (1,2-dimyristoyl-*sn*-glycero-3-phosphocholine) nanoliposome-encapsulated curcumin and pure curcumin after 60 days, respectively, implying better pharmacokinetic properties of the curcumin modified with DMPC nanoliposomes [53]. Song et al. research revealed that there was an enhancement in solubility of the curcumin and an herbal compound named tetrandrine after either of them was subjected to the liposomes prepared from soybean lecithin and cholesterol, together with a stabilizer called DSPE-MPEG 2000 [24]. Wang et al. encapsulated Bis into D- α -tocopherol polyethylene glycol 1000 succinate (TPGS) liposomes, bringing about high percentage of encapsulation efficiency, percentage of loading capacity, and oral bioavailability [54]. The study of Yeh et al. showed high percentage of encapsulation efficiency in both Cu- and Bis-loaded soybean phosphatidylcholine (SPC) liposomes [55]. For using multiple curcuminoids, Panichayupakaranant et al. ameliorated the pharmacokinetic properties of a combination of Cu, De, and Bis. Initially, dried *Curcuma longa* L. powders were processed to derive CRE, containing 88% w/w of the preceding curcuminoids. Then, by utilizing solid dispersion, the CRE was incorporated with PVP K30 to obtain the CRE-SD, comprising 7% w/w curcuminoids [56-58].

1.2.5 NF- κ B signaling pathway

Major component proteins of the NF- κ B signaling pathway

In NF- κ B signaling pathway of mammalian cells, the main component proteins can be divided into 3 groups [25,27,29]:

1. NF- κ B transcription factors, including p65 (Rel A), Rel B, c-Rel, p105 (NF- κ B1), and p100 (NF- κ B2). These five proteins have N-terminal Rel homology region or Rel homology domain (RHR or RHD) functioning in binding to DNA, dimerization, and binding to inhibitory proteins (e.g., I κ B proteins). Within the RHD of all NF- κ B transcription factors, there is a nuclear localization sequence (NLS). Following the RHD sequence, there is a transactivation domain (TAD; containing

binding sites for other proteins) in p65, Rel B, and c-Rel, as opposed to the presence of C-terminal ankyrin repeats (AnkRs) in p105 and p100. The post-translational cleavage or proteolysis of AnkRs of precursor proteins (p105 and p100) gives rise to p50 and p52, respectively. p65, Rel B, c-Rel, p50, and p52 can form homodimers or heterodimers, which the most common form is p65/p50 heterodimer. The heterodimers consisting of p65, Rel B, or c-Rel monomer are transcriptional activators, whereas p50/p50 and p52/p52 homodimers act as repressors except those that bind to secondary proteins.

2. I κ B proteins, comprising I κ B α , I κ B β , I κ B ϵ , BCL-3, I κ Bz, I κ BNS, I κ B γ (NEMO), and I κ B δ . The last two proteins are the C-terminal portion of p105 and p100, respectively. All eight I κ B proteins have 5-7 tandem AnkRs, which can bind to NF- κ B transcription factors covering the NLS.

3. protein subunits of IKK complex, including at least a noncatalytic regulatory subunit named NEMO and two catalytic kinase subunits (IKK α (IKK1) and IKK β (IKK2)).

Canonical and noncanonical NF- κ B signaling pathways

The RANKL-RANK upstream signaling pathway of osteoclasts activates canonical and noncanonical (alternative) downstream NF- κ B signaling pathways, together with osteoclast differentiation [28]. The key information of both NF- κ B signaling pathways can be summarized in Table 3 and Figure 4-5.

Table 3 Comparison between canonical and noncanonical NF- κ B signaling pathways

	Canonical NF- κ B signaling pathway	Noncanonical NF- κ B signaling pathway
Response	respond rapidly and transiently to manifold external stimuli involving inflammation, immune response, cell proliferation, cell differentiation, and cell survival	respond slowly and persistently for specific biological functions in the immunological mechanisms
Upstream receptors/protein complex	tumor necrosis factor (TNF) receptors (e.g., RANK, etc.), T-cell receptors (TCRs), toll-like receptors (TLRs), and	TNF superfamily receptors (e.g., RANK, lymphotoxin β receptors (LT β R), B-cell activating factor receptors (BAFF-Rs), CD40, CD27,

	Canonical NF-κB signaling pathway	Noncanonical NF-κB signaling pathway
	interleukin 1 receptors, type I (IL-1RI)	etc.), complement membrane attack complex (MAC)
Mechanism	<p>The stimulated upstream signaling pathway results in the activation of the cytoplasmic adaptor molecules in the NF-κB signaling pathway. Subsequently, adaptor molecules activate IKKβ and IKKα of IKK complex to phosphorylate IκBα and p65 of the IκBα/p50/p65 protein complex, respectively. Next, there are the polyubiquitination and degradation of p-IκBα by the 26S proteasome.</p> <p>The p50/p65 heterodimer – the NF-κB dimer form which has the most structural stability – freely translocates to the nucleus for the transcription of target genes.</p>	<p>1. The stimulated upstream signaling pathway via ligand-receptor interactions leads to the activation and stabilization of NF-κB-inducing kinase (NIK). Thereafter, activated NIK phosphorylates IKKα of the IKKα homodimer. This brings about the phosphorylation of p100, along with the conversion of p100 of p100/Rel B heterodimer into p52 (by the ubiquitination and proteolysis of Anks of p100). Finally, the nuclear translocation and the subsequent transcription of p52/Rel B heterodimer are proceeded.</p> <p>2. The activation of MAC causes the production of endosomes consisting of NIK, AKT and MAC proteins. These endosomes modulate aforesaid NIK stabilization and IKKα phosphorylation.</p>

NOTE: The information in the table is referred from [25-30].

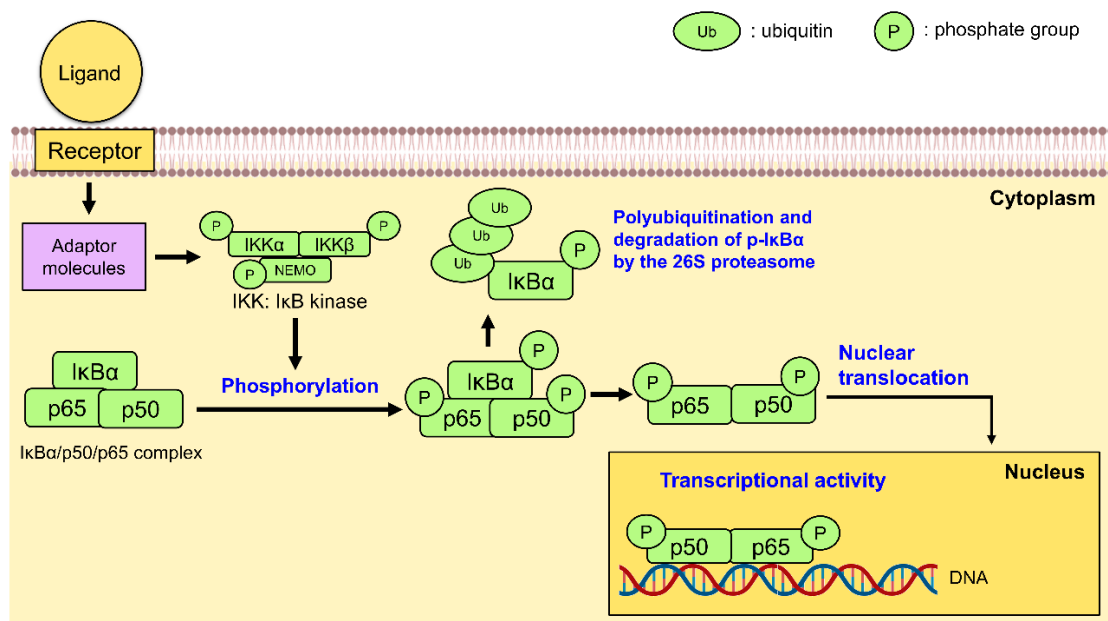


Figure 4 Canonical NF-κB signaling pathway

The figure is adapted from [28,30].

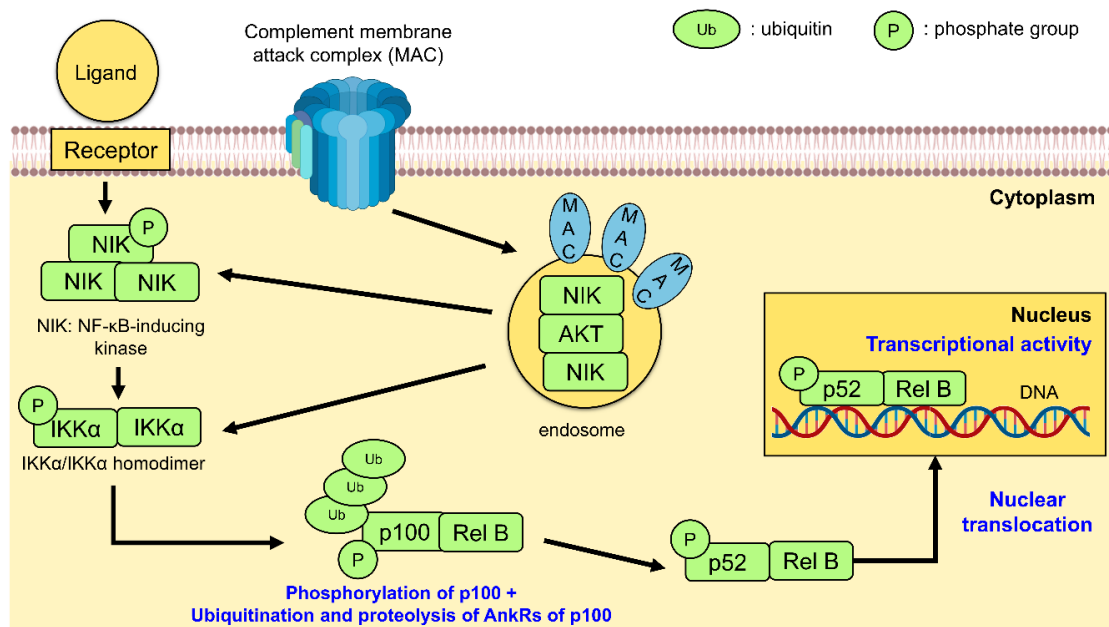


Figure 5 Noncanonical NF-κB signaling pathway

The figure is adapted from [28,30].

Throughout the thesis, the canonical NF-κB signaling pathway, which is in the thesis scope, will be mainly focused.

The modulatory effect of curcuminoids on osteoclastogenesis via canonical NF-κB signaling pathway

Recent studies have substantiated the potential of curcuminoids to inhibit the osteoclastogenesis via canonical NF-κB signaling pathway. Chauhan et al. review illustrated that the curcumin can suppress the IκBα phosphorylation and degradation, together with the nuclear translocation of p65 [31]. Bharti et al. and Yang et al. demonstrated the inhibitory effect of curcumin on RANKL-RANK upstream and canonical NF-κB downstream signaling pathways (i.e., the decreased phosphorylation of IκBα and p65) of RANKL-stimulated murine RAW 264.7 macrophages (osteoclasts) [32,33]. Pengjam et al. proved that CRE-Ter (CRE ternary complex modified with PVP K30 and HPBCD) may have a suppressive effect on the RANKL-stimulated murine RAW 264.7 cell differentiation by reducing the p65 and IκBα phosphorylation [59]. Moreover, the POPC liposomes encapsulating CRE-Ter can inhibit the differentiation of the RANKL-stimulated murine RAW 264.7 cells by downregulating the p65 phosphorylation [60].

The involvement of reactive oxygen species (ROS) in NF- κ B signaling pathway and osteoclastogenesis

ROS – containing reactive oxygen molecules and oxygen free radicals, e.g., superoxide anions, hydrogen peroxide, and hydroxyl radicals – are crucial intracellular secondary messengers for diverse cellular mechanisms [61,62]. Many previous reports revealed that the ROS can be a stimulating and inhibiting factor of canonical and noncanonical NF- κ B signaling pathways as well as a regulator of promoting osteoclast differentiation [61-64]. Additionally, the immoderate ROS production leads to the oxidative stress (an imbalance between the ROS and antioxidant in the cells), inducing excessive osteoclast differentiation/bone resorption, and bone diseases [61]. As mentioned, curcuminoids have antioxidant property. Previous investigation stated that the curcuminoids are capable for the elimination of the free radicals [65]. This suggests that the curcuminoids possibly suppress canonical and noncanonical NF- κ B signaling pathways and consequent osteoclastogenesis by modulating the ROS.

1.2.6 Molecular docking simulation

Main concept of molecular docking simulation

Protein–ligand molecular docking simulation is a computer-aided drug design (CADD) approach for predicting the 3D binding pose (the most possible orientation and conformation of a ligand when it binds to the receptor protein). This computational technique fulfills the elucidation of the protein–ligand interactions and the related biomolecular mechanisms, apart from *in vitro/in vivo* experiments and clinical trials. For example, the interactions between IL-6 (protein data bank (PDB) ID: 4NI9) and MD2-TLR4-IN-1 (IL-6 inhibitor ligand; PubChem compound identifier (CID): 138454798) reported by Oh et al. [10], along with the interactions between CTSK (PDB ID: 4DMY) and CTSK inhibitors revealed by Xue et al. [11]. Integrating the docking results with other pharmacological data and/or experimental findings may show the suppressive effect of the preceding ligands to treat bone diseases [10,11]. In terms of novel drug discovery, molecular docking simulation can minimize the immoderate cost and time from conducting wet-lab binding affinity measurements of numerous ligands, which only some of them can be the plausible drug candidates [66,67]. The docking process uses scoring function – the mathematical function applied for binding affinity prediction [68]. After finishing the docking, the binding regions are displayed as cubic boxes with the specific center and size [69]. Moreover, the calculated scores computed from the scoring function are ranked and derived.

A type of protein–ligand docking named blind docking is the process of predicting protein–ligand interactions by performing on the entire protein surface [69]. Since the traditional blind docking may have low reliability and stability thanks to large docking space, many blind docking tools have combined protein binding site prediction module, especially binding pocket (cavity) detection, with the docking modules. This

development may contribute to the accurate and cost-effective blind docking [69]. In this thesis, CB-Dock 2 – web-based protein–ligand blind docking tool – was implemented to analyze the interactions between the curcuminoids and the I κ B α /p50/p65 complex. The description and the docking procedure of CB-Dock 2 are explained in Chapter 2.

Molecular docking simulation between curcuminoids and major proteins in the canonical NF- κ B signaling pathway

Recently, the molecular docking simulation between Cu/De/Bis and main proteins in the canonical NF- κ B signaling pathway is understudied. Cheemanapalli et al. identified the active sites (binding pockets) of IKK complex (PDB ID: 3BRV), proteasome (PDB ID: 1D3Z), p65 (PDB ID: 1NFI), and NF- κ B (p105/p65 protein complex; PDB ID: 3GUT) by using the Computed Atlas of Surface Topography of Proteins (CASTp) program. Then, the molecular docking simulation between curcumin and each of the proteins was performed by using the AutoDock program version 4.0. The findings showed the highest pocket surface area and the highest pocket volume of the binding pocket of NF- κ B, among all four proteins. Furthermore, the information on the docking output revealed the binding interactions between curcumin and specific amino acid residues of the active sites of all four proteins. The lowest binding energies of IKK complex, proteasome, p65, and NF- κ B were -4.13 , -4.38 , -6.00 , and -5.42 kcal/mol, respectively [34]. Saeed et al. implemented AutoDock program version 4.2.6 for molecular docking simulation between 50 curcumin compounds (including Cu, De, Bis, etc.) and the p50/p65 heterodimer complexed to the I κ B DNA (PDB ID: 1IVX). The calculated means of binding energies of Cu, De, and Bis (-8.38 ± 0.16 , -8.07 ± 0.10 , and -7.96 ± 0.05 kcal/mol, respectively) indicated strong binding affinity between the protein complex and the curcuminoids [35].

1.2.7 Discussion

Manifold previous *in vitro* and *in vivo* studies confirmed the performance of Cu, De, and Bis to inhibit immoderate osteoclastogenesis via canonical NF- κ B pathway, implying the capability of the curcuminoids to prevent excessive bone resorption and bone diseases. Solid dispersion and liposome encapsulation have been utilized to ameliorate the pharmacokinetic properties of the curcuminoids. Additionally, molecular docking simulation suggested the molecular interactions between the curcuminoids and the major proteins in canonical NF- κ B pathway. However, whether the pharmacokinetic attributes enhance after applying liposome encapsulation to the CRE-SD remains unclarified. The *in vitro* inhibitory effect of the liposomal CRE-SD on osteoclast differentiation via canonical NF- κ B pathway is not elucidated. Apart from that, the molecular interactions between Cu/De/Bis and I κ B α /p50/p65 protein complex are not fully elucidated. To address these knowledge gaps, the characterization of the liposomal CRE-SD, the examination of *in vitro* release

of the liposomal CRE-SD, the *in vitro* experiments, and molecular docking simulation were conducted in this study.

1.3 Objectives

1. To evaluate the characteristics and *in vitro* release of the liposomal CRE-SD.
2. To analyze the biomolecular regulation of liposomal CRE-SD on osteoclastogenesis via the canonical NF- κ B pathway by performing *in vitro* experiments.
3. To analyze the molecular interactions between the I κ B α /p50/p65 protein complex and Cu/De/Bis by performing molecular docking simulation.

CHAPTER 2

RESEARCH METHODOLOGY

2.1 *In vitro* experiments

2.1.1 Cells and reagents

Murine RAW 264.7 macrophages were purchased from the ATCC Cell Bank (Biomedica, Bangkok, Thailand). RANKL was purchased from R&D Systems (Minneapolis, USA). RPMI 1640 cell culture medium was purchased from Gibco Co. (Bangkok, Thailand). The RNeasy kit for RNA extraction was purchased from Qiagen (Valencia, CA, USA). The other chemicals mentioned in the study were purchased from Sigma Chemical Co. (Bangkok, Thailand).

2.1.2 Preparation, characterization, and *in vitro* release of liposomal CRE-SD

CRE containing 88% *w/w* total curcuminoids (72.81% \pm 0.83% *w/w* Cu, 12.49% \pm 0.57% *w/w* De, and 4.24% \pm 0.16% *w/w* Bis; the curcuminoid content was measured by Lateh et al. using HPLC analysis [57]) and CRE-SD containing 7% *w/w* curcuminoids were prepared using the method described by Lateh et al. [57,58]. The dried powder of *C. longa* rhizomes was dissolved in ethanol, and microwave-assisted extraction was performed (900 W and three irradiation cycles; each cycle comprised 3 min on followed by 30 s off). Then, the filtration and elution of the resulting *C. longa* extracts were conducted to derive CRE. For the latter process, a Diaion[®] HP-20 column (Mitsubishi Chemical Co., Tokyo, Japan) with the incorporation of 55% and 60% *v/v* ethanol was utilized. To obtain CRE-SD, PVP K30 (10% mass ratio) was mixed with CRE, and solvent evaporation of the CRE mixture was performed under reduced pressure.

The liposomal suspension (25 mol 1-palmitoyl-2-oleoyl-phosphatidylcholine (POPC):1 mol CRE-SD in phosphate-buffered saline (PBS); pH 7.4) was prepared in accordance with the procedure reported by Sinjari et al. [52]. A POPC aliquot (Avanti Polar Lipids, Alabama, USA) was first dissolved in chloroform. Then, the aliquot was transferred to a round-bottomed flask and dried in a rotary evaporator (low pressure, 40 °C). A phospholipid film formed on the inner wall of the flask. This film was stored overnight at 4 °C, rehydrated with PBS buffer (pH 7.4), and sonicated for 30 min. The resulting liposome suspensions were sterilized for 2 h under a UV lamp. Finally, an appropriate quantity of CRE-SD, dissolved in dimethylsulfoxide, was added to the suspensions.

To evaluate the characteristics of the liposomes, i.e., the liposome hydrodynamic diameter, polydispersity index (PDI), and zeta potential at pH 7.4, the procedure described by Pengjam et al. was applied [60]. The liposomal diameter and

PDI were measured using dynamic light scattering (DLS) via a Zetasizer Nano-S instrument (Malvern Instruments, Malvern, UK). To derive the surface charge of the liposomes, their electrophoretic mobility (μ) was measured using correlation spectroscopy via a Zetasizer Nano-S instrument. The Smoluchowski equation, $Z = \mu\eta/\varepsilon$, was used to calculate the zeta potential (Z), where η and ε indicate viscosity and solution permittivity, respectively. All measurements were performed at room temperature, and 200 μ L of each sample was diluted 20-fold in a citric-phosphate buffer solution.

The *in vitro* release of CRE-SD was assessed using the method stated by Pengjam et al. [60]. The overnight immersion of dialysis tubing (molecular weight cutoff: 12,000–14,000 Da; Carolina Biological Supply Company (NC, USA)) was performed in deionized water to remove preservatives. A dialysis sac with CRE-SD and another dialysis sac with liposomal CRE-SD were employed. After the dialysis sacs were sealed, PBS (pH 7.4) was dissolved in 25% *v/v* methanol in a flask using a glass stirring rod. Then, the flask, maintained at 37.0 ± 0.1 °C, was stirred constantly with a magnetic stirrer at 150 rpm. The mass of CRE-SD leaked from each sac was measured every 10 days, from day 0 to day 70. Then, the cumulative mass percentage of CRE-SD released at each timepoint was derived using the following formula:

$$\% \text{ cumulative mass of released CRE-SD on day } (10 \times (n-1)) = \frac{\sum_{i=1}^n m_i}{M_{\text{CRE-SD}}} \times 100\%$$

where n represents the timepoint of the measurement, ranging from 1 to 8, i.e., days 0, 10, ..., 70, respectively; $\sum_{i=1}^n m_i$ denotes the summation of the masses of the leaked CRE-SD from timepoint 1 to timepoint n ; and $M_{\text{CRE-SD}}$ indicates the mass of the CRE-SD incorporated to the dialysis sac on day 0.

2.1.3 Culture of RAW 264.7 cells

RAW 264.7 cells were grown in RPMI 1640 medium, supplemented with 10% heat-immobilized fetal bovine serum (FBS), 100 U/mL penicillin G, 2 mM glutamine, and 100 μ g/mL streptomycin sulfate. The cells were incubated in a cell culture vessel at 37 °C under humid conditions and 5% carbon dioxide. At the subconfluent stage, when approximately 70–80% of the surface of the cell culture vessel was occupied, the cells were harvested, following the application of 0.25% trypsin and 0.02% ethylenediaminetetraacetic acid. Then, 5×10^3 RAW 264.7 cells were seeded into each well of a culture plate for the subsequent *in vitro* experiments. The culture medium (RPMI 1640 containing supplements) was replenished every 3 days.

2.1.4 Evaluation of optimal RANKL incubation time in RAW 264.7 cells treated with CRE-SD-free POPC liposomes (CRE-SD-FREE-LIP)

To investigate the optimal RANKL incubation time, RAW 264.7 cells with and without 20 ng/mL RANKL treatments were incubated with CRE-SD-FREE-

LIP for 1, 2, 3, 4, and 5 days. A TRAP assay was performed to detect TRAP activity. The TRAP assay kit was purchased from TaKaRa Bio Inc., Tokyo, Japan. The relative expression of CTSK was measured using the qRT-PCR procedure described by Pengjam et al. [60].

2.1.5 Viability examination of liposomal CRE-SD-treated RAW 264.7 cells

RAW 264.7 cells were classified into two groups: RANKL-stimulated RAW 264.7 cells, which were subjected to 20 ng/mL RANKL for 5 days; and RAW 264.7 cells without RANKL stimulation. CRE-SD-FREE-LIP and liposomal CRE-SD (1, 2.5, 5, 10, 20, and 30 $\mu\text{g/mL}$) were added to the cultured cells. Thereafter, an MTT assay was conducted to examine viable cells. The absorbance of each cell sample at 570 nm was measured using a Thermo Scientific spectrophotometer (Multiskan FC, Pittsburgh, PA, USA). Thereafter, the resulting absorbance was converted into the number of viable cells.

2.1.6 Confirmation of osteoclastogenic inhibition in liposomal CRE-SD-treated RANKL-stimulated RAW 264.7 cells

For the TRAP staining assay, RANKL-unstimulated RAW 264.7 cells, along with 20 ng/mL RANKL-stimulated RAW 264.7 cells with CRE-SD-FREE-LIP and 20 $\mu\text{g/mL}$ liposomal CRE-SD, were incubated for 5 days in a cell culture vessel under the previously described conditions. On day 5, TRAP staining was performed, and the morphology of the cells was subsequently observed under a brightfield light microscope at 1000 \times magnification. Purplish to dark red granules in the cytoplasm denoted the presence of intracellular TRAP. The percentage of multinucleated TRAP-positive cells, i.e., the cells containing stained granules, was calculated.

To measure TRAP activity, 20 ng/mL RANKL-stimulated RAW 264.7 cells were incubated with CRE-SD-FREE-LIP and liposomal CRE-SD (5, 10, and 20 $\mu\text{g/mL}$) for 5 days. After cell culture, the TRAP activity was measured using the TRAP assay kit, as previously described.

To examine F4/80 expression, RANKL-unstimulated RAW 264.7 cells, along with 20 ng/mL RANKL-stimulated RAW 264.7 cells with CRE-SD-FREE-LIP and 20 $\mu\text{g/mL}$ liposomal CRE-SD, were incubated for 5 days under the previously described cell culture conditions. As the anti-F4/80 antibody can interact with the F4/80 antigen, a murine macrophage marker [70], immunocytochemical staining for anti-mouse F4/80 antibody, using method reported by Pengjam et al. [60], was performed to analyze the expression of F4/80, which was representative of the abundance of murine macrophages in each sample. The following steps were conducted at room temperature. Each cell sample was rinsed in PBS and subsequently fixed for 10 min in 4% paraformaldehyde dissolved in PBS. Subsequently, 0.3% hydrogen peroxide in absolute methanol was added to the samples for 15 min to inhibit the cellular

endogenous peroxidase activity. Then, the samples were preincubated for 1 h with 500 µg/mL normal goat IgG antibody dissolved in 1% BSA in PBS (pH 7.4). The samples were incubated for 2 h with anti-mouse F4/80 antibody, washed with 0.075% Brij 35 in PBS, and then incubated for 1 h with horseradish peroxidase (HRP)-conjugated goat anti-mouse IgG antibody in 1% BSA in PBS. They were further washed with 0.075% Brij 35 in PBS. Then, under dark conditions, the cells were exposed to the substrate 3,3'-diaminobenzidine (DAB), along with a nickel and cobalt solution (DAB enhancer). Regarding the reaction catalyzed by the HRP, the DAB oxidized by hydrogen peroxide resulted in the formation of brown patches. Finally, the cell samples were mounted onto glass slides, and microscopic images were captured using an Olympus brightfield light microscope and a digital camera. At 1000× magnification, brown patches in the microscopic images indicate stained murine macrophages, hereafter referred to as F4/80-positively stained cells. Additionally, the percentage of F4/80-positively stained cells was computed. RAW 264.7 cells treated with CRE-SD-FREE-LIP without RANKL stimulation were used as the control.

To detect the expression of osteoclast marker genes, 20 ng/mL RANKL-treated RAW 264.7 cells exposed to CRE-SD-FREE-LIP and liposomal CRE-SD (10 and 20 µg/mL) were incubated for 5 days under the previously described cell culture conditions. Then, the relative expressions of the CTSK, c-Fos, and NFATc1 genes were measured using RT-PCR. Total RNA was extracted using an RNeasy Mini Kit (Qiagen, USA), and complementary DNA was synthesized using a ReverTra Ace qPCR kit (Toyobo, Osaka, Japan). A Fast-Start SYBR Green Master Mix and a BIOER LifeECO™ PCR Thermal Cycler (Bangkok, Thailand) were utilized for RT-PCR amplification. The amplicons were then transferred to a Mupid-EXU Gel Electrophoresis System (Bangkok, Thailand) for agarose gel electrophoresis. Images of the gels were captured using a UVITEC Gel Documentation System (Bangkok, Thailand) and analyzed using a Bio-Rad ChemiDoc MP Imaging System (Bangkok, Thailand).

2.1.7 Primer sequences for RT-PCR and qRT-PCR amplification

The primer sequences used for RT-PCR and qRT-PCR are shown below:

CTSK	Forward: 5' ATGTGGGGGCTCAAGGTTCTG 3'
	Reverse: 5' CATATGGGAAAGCATCTTCAGAGTC 3'
c-Fos	Forward: 5' CCAGTCAAGAGCATCAGCAA 3'
	Reverse: 5' AAGTAGTGCAGCCCGGAGTA 3'
NFATc1	Forward: 5' CCGTTGCTTCCAGAAAATAACA 3'
	Reverse: 5' TGTGGGATGTGAACTCGGAA 3'

GAPDH (internal control)

Forward: 5' AAATGGTGAAGGTCGGTGTG 3'

Reverse: 5' GAATTTGCCGTGAGTGGAGT 3'

2.1.8 Detection of phosphorylation of p65 and I κ B α proteins in liposomal CRE-SD-treated RANKL-stimulated RAW 264.7 cells

Western blotting was used to detect the phosphorylation of p65 and I κ B α . First, RAW 264.7 cells stimulated with 20 ng/mL RANKL were exposed to CRE-SD-FREE-LIP and liposomal CRE-SD (10 and 20 μ g/mL) for 5 days. Cytoplasmic and nuclear protein extraction were performed using the NE-PER reagent (Thermo Scientific Inc., Washington, DC, USA) in accordance with the manufacturer's protocol. Subsequently, SDS-PAGE was used to separate proteins. Then, the separated proteins were blotted onto polyvinyl difluoride membranes. Nonspecific binding to the membrane was blocked prior to incubation with the following primary antibodies, which were purchased from Cell Signaling Technology (Beverly, MA, USA): anti-p65, anti-phosphorylated p65, anti-I κ B α , anti-phosphorylated I κ B α , and anti- β -actin antibodies. The membrane was washed to eliminate unbound antibodies, and then incubated for 1 h with HRP-conjugated secondary antibodies. The membrane was washed again. Finally, a Bio-Rad ChemiDoc MP Imaging System (Bangkok, Thailand) was employed to detect the protein bands on the membrane.

2.1.9 Confirmation of the inhibitory effect of liposomal CRE-SD on nuclear translocation and transcriptional activity of phosphorylated p65 (p-p65)

To confirm whether liposomal CRE-SD impedes nuclear translocation and the transcriptional activity of p-p65, subconfluent RAW 264.7 cells were treated for 4 h with 20 ng/mL RANKL and JSH23 (4-methyl-N1-(3-phenylpropyl)-1,2-benzenediamine; IC₅₀ = 7.1 μ M), an inhibitor of NF- κ B nuclear translocation and transcriptional activity. The cells were then incubated for 16 h with 20 μ g/mL liposomal CRE-SD. Next, the cell lysates were collected using the approach described by Pengjam et al. [59]. Finally, Western blotting was performed as described in Section 2.1.8. RANKL-stimulated RAW 264.7 cells treated with CRE-SD-FREE-LIP were used as the control.

2.1.10 Detecting intracellular ROS production

To analyze the effect of liposomal CRE-SD on intracellular ROS production in RANKL-stimulated RAW 264.7 cells, an OxiselectTM Intracellular ROS assay kit (CellBio Lab, Inc., San Diego, CA, USA) was employed. First, 20 ng/mL RANKL-stimulated RAW 264.7 cells were incubated for 12 h with CRE-SD-FREE-LIP and liposomal CRE-SD (5, 10, and 20 μ g/mL), along with 10 μ M 2',7'-

dichlorofluorescein diacetate. Next, the fluorescence signal from 2',7'-dichlorofluorescein (DCF) in each cell sample was measured at excitation and emission wavelengths of 485 and 530 nm, respectively, using a spectrofluorometer (Beckman Coulter, Inc., CA, USA). As the intracellular ROS concentration is proportional to the signal intensity of DCF, the percentage of intracellular ROS production was calculated based on the signal intensity.

2.1.11 Statistical analysis

All numerical data are expressed as the mean \pm SD ($n = 3$). Statistical analyses were performed using one-way analysis of variance, the post hoc Dunnett's test, and the Student's *t*-test. *p*-values of < 0.05 were considered to indicate statistical significance.

2.2 *In silico* analyses

2.2.1 Retrieval of the structures of the I κ B α /p50/p65 complex and curcuminoids

The 3D structure of the I κ B α /p50/p65 complex (PDB ID: 1IKN) was retrieved from RCSB PDB (<https://www.rcsb.org/>, accessed on 21 December 2022) [71] in PDB format. The 1IKN file comprises p65 (chain A), p50D (chain C), and I κ B α (chain D) subunits. The 3D chemical structures of Cu, De, and Bis (PubChem CIDs: 969516, 5469424, and 5315472, respectively) were retrieved from the PubChem database (<https://pubchem.ncbi.nlm.nih.gov/>, accessed on 20 December 2022) [72] in SDF format.

2.2.2 Blind docking simulation between the I κ B α /p50/p65 complex and Cu/De/Bis

CB-Dock2, a web-based blind docking simulation tool (<https://cadd.labshare.cn/cb-dock2/php/index.php>, accessed on 25 January 2023) [73], was employed for protein–ligand blind docking. After submitting the ligand and protein structure files to CB-Dock2, the chemical structures were assessed. The RDKit in CB-Dock2 adds hydrogens and partial charges to the uploaded ligand chemical structure. Furthermore, RDKit generates an initial 3D ligand conformation. Then, CB-Dock2 amends the uploaded protein structure by adding missing hydrogen atoms as well as residues and removing heteroatoms (atoms that do not belong to the protein), as well as co-crystallized water molecules. Next, a protein surface curvature-based cavity detection method, known as CurPocket, was used for binding pocket (cavity) detection. CurPocket identifies the five largest binding pockets, as well as the docking parameters (e.g., grid center coordinates, size, and volume of the docking box (search space)), of the uploaded protein. After the retrieval of the binding pocket profile and selection of

the docking cavities, structure-based ligand–protein blind docking, with or without template-based ligand–protein blind docking, was executed. The former is mandatorily performed via the AutoDock Vina (version 1.1.2) algorithm, whereas the latter is conducted using FitDock when the query protein–ligand complex is homologous to the known protein–ligand complex in the BioLip database (i.e., FP2 fingerprint of ≥ 0.4 (high topology similarity), sequence identity of the binding pocket of $\geq 40\%$, and structure root mean squared deviation (RMSD) of the binding pocket of ≤ 4 Å). Finally, the blind docking information regarding the optimal binding site and binding pose (the candidate of binding mode (the orientation and conformation of the ligand that binds to the protein)) of the ligand, as well as the Vina/FitDock scores, are displayed. The superior performance of CB-Dock2 was corroborated through the 85.9% success rate of the top-ranking binding mode (RMSD of ≤ 2 Å) prediction, which was much higher than those achieved using other docking algorithms (CB-Dock, FitDock, MTiAutoDock, SwissDock, and COACH-D) [73].

Therefore, a blind docking simulation was conducted to explore the optimal binding site and binding pose of each curcuminoid (Cu/De/Bis) to the I κ B α /p50/p65 complex. Initially, the 1IKN PDB file and the SDF files of each curcuminoid were uploaded to the CB-Dock2 web server to identify the five largest binding pockets. Then, all five cavities were used for blind docking. As the query and template ligand–protein complexes do not match, only structure-based blind docking was utilized. Finally, for each curcuminoid, the docking simulation result with the most negative Vina score, which indicates the strongest binding affinity, was analyzed to derive the binding pose, docking space (docking center and docking size), possible contact residues, and molecular interactions. The binding pose, contact residues, and molecular interactions were visualized using BIOVIA discovery studio visualizer (version 21.1.0.20298; <https://discover.3ds.com/discovery-studio-visualizer-download/>, accessed on 13 February 2023).

CHAPTER 3

RESULTS

3.1 Liposomal CRE-SD characterization

The suspensions of CRE-SD-FREE-LIP and liposomal CRE-SD were prepared. The liposomal characteristics—liposome diameter, PDI, and zeta potential at pH 7.4—measured from both liposomal suspensions are shown in Table 4.

Table 4 Liposomal characteristics

Liposome suspension	Liposome diameter (nm)	Polydispersity index (PDI)	Zeta Potential at pH 7.4 (mV)
CRE-SD-FREE-LIP	328.0 ± 14.5	0.45 ± 0.11	-22.22 ± 0.51
Liposomal CRE-SD	380.1 ± 20.5	0.43 ± 0.13	-31.00 ± 0.48

3.2 *In vitro* assessment of CRE-SD release

To analyze the *in vitro* release of CRE-SD, a dialysis sac with CRE-SD and a dialysis sac with liposomal CRE-SD were studied and compared. The mass of CRE-SD released was measured and the cumulative mass percentages were calculated. As illustrated in the 70-day CRE-SD release profile (Figure 6), the proportion of the cumulative mass of released CRE-SD in CRE-SD samples increased sharply, from 2.0% ± 1.2% on day 0, to 32.1% ± 1.3% on day 30. Thereafter, it increased slightly to 36.1% ± 1.0% on day 70. In contrast, the proportion in liposomal CRE-SD samples ranged from 1.0% ± 0.8% on day 0, to 7.0% ± 1.0% on day 70, and did not dramatically change over the 70-day measurement period.

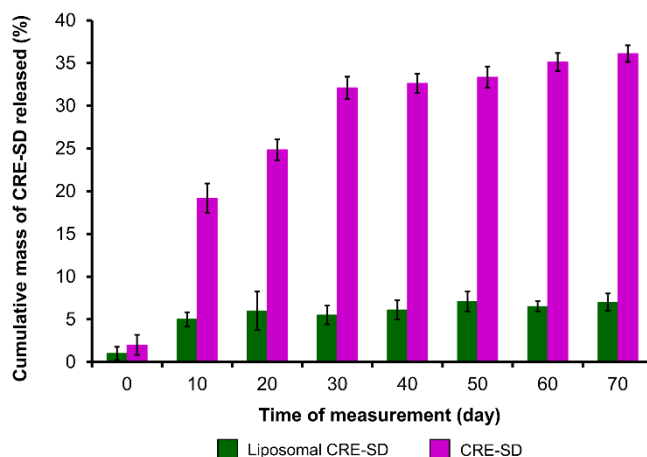


Figure 6 *In vitro* assessment of CRE-SD release after liposomal encapsulation

The percentages of the cumulative mass of CRE-SD released in liposomal CRE-SD and CRE-SD samples were measured from day 0 to 70, every 10 days ($n = 3$).

3.3 Optimization of RANKL incubation time

The optimal RANKL incubation time was investigated by detecting TRAP activity and CTSK relative expression of murine RAW 264.7 macrophages treated with CRE-SD-FREE-LIP (Figure 7A–B). In cells that were not treated with 20 ng/mL RANKL, no significant changes were found throughout the 5-day incubation period. In contrast, in the 20 ng/mL RANKL-treated cells, the TRAP activity increased significantly on days 3–5, and the CTSK relative expression was significantly elevated on days 4 and 5.

3.4 Optimization of liposomal CRE-SD concentration

CRE-SD-FREE-LIP and liposomal CRE-SD (1, 2.5, 5, 10, 20, or 30 $\mu\text{g/mL}$) were added to RAW 264.7 cells with and without 20 ng/mL RANKL treatments for 5 days. Then, an MTT assay was performed to assess the number of viable cells in each cell sample and explore the most effective liposomal CRE-SD concentration that did not induce cytotoxicity. As shown in Figure 7C, the number of viable cells significantly decreased after RANKL-stimulated RAW 264.7 cells were exposed to 30 $\mu\text{g/mL}$ liposomal CRE-SD. The RANKL-stimulated and -unstimulated RAW 264.7 groups treated with up to 20 $\mu\text{g/mL}$ liposomal CRE-SD had greater numbers of viable cells than did the group treated with CRE-SD-FREE-LIP, indicating the proliferative effect of liposomal CRE-SD. However, there was no statistically significant difference in the number of viable cells.

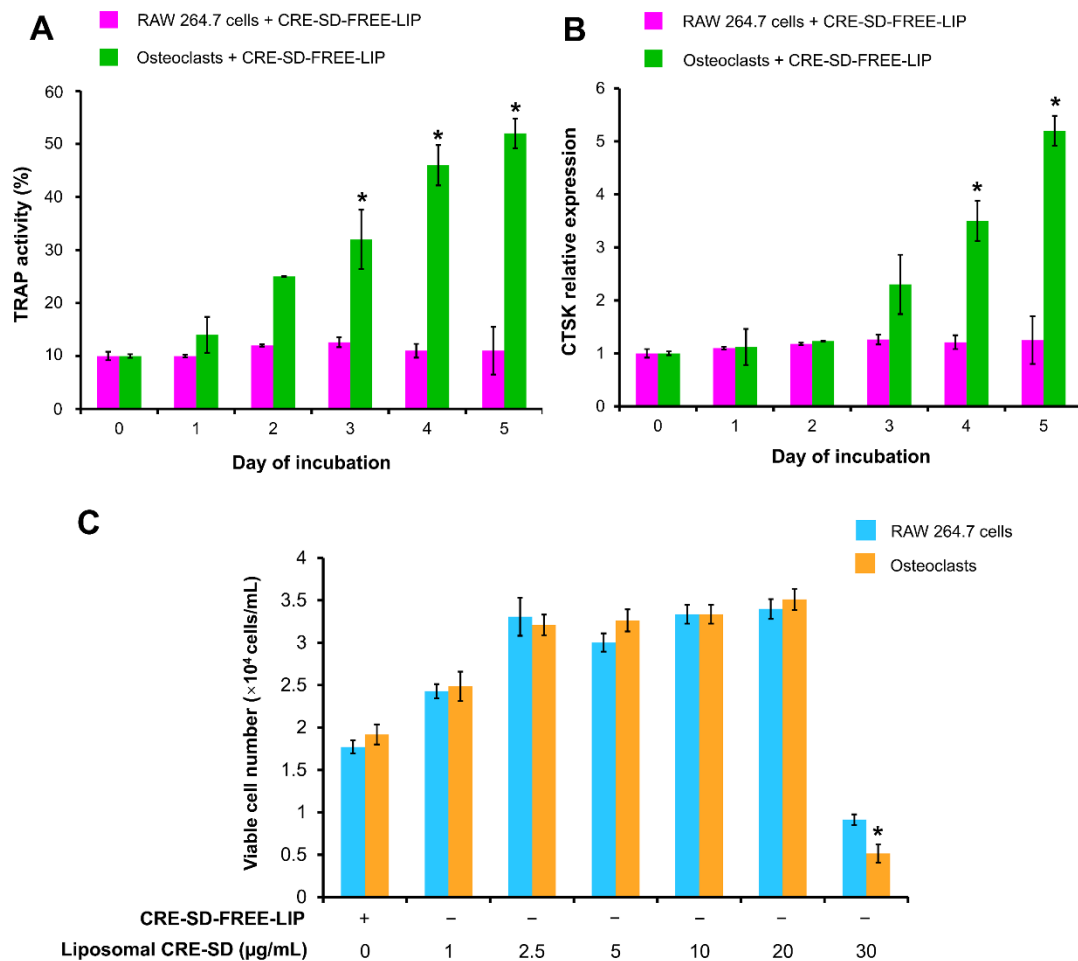


Figure 7 Optimization of RANKL incubation time and liposomal CRE-SD concentration

In the first study, RAW 264.7 cells were treated with 20 ng/mL RANKL and CRE-SD-free POPC liposomes (CRE-SD-FREE-LIP) for 1, 2, 3, 4, and 5 days to detect (A) TRAP activity and (B) the relative expression of cathepsin K (CTSK). Statistically significant differences in cell samples between any incubation day and incubation day 0 are indicated with an asterisk (*). In the second study, RAW 264.7 cells were treated with CRE-SD-FREE-LIP and liposomal CRE-SD (1, 2.5, 5, 10, 20, and 30 µg/mL) and incubated for 5 days with and without 20 ng/mL RANKL to estimate (C) the number of viable cells. Statistical significance of the difference between the corresponding liposomal CRE-SD-treated and CRE-SD-FREE-LIP-treated samples is denoted as * $p < 0.05$, $n = 3$.

3.5 Inhibitory effect of liposomal CRE-SD on osteoclastogenesis

To explain the liposomal CRE-SD effect on osteoclastogenesis, morphological examinations were performed, the proportions of multinucleated TRAP-positive cells and F4/80-positively stained cells were calculated, and the expression of

osteoclast markers was detected. Initially, TRAP staining and a TRAP assay were used to examine the RAW 264.7 cell samples. The microscopic images indicated the existence of multinucleated TRAP-positive cells in 20 ng/mL RANKL-stimulated RAW 264.7 cell samples with CRE-SD-FREE-LIP and 20 μ g/mL liposomal CRE-SD (Figure 8A and Figure A1). The percentage of multinucleated TRAP-positive cells in the 20 μ g/mL liposomal CRE-SD-treated samples was significantly lower than that in the CRE-SD-FREE-LIP-treated samples (Figure 8B). Subsequently, the TRAP activities of 20 ng/mL RANKL-stimulated RAW 264.7 cell samples treated with various concentrations of liposomal CRE-SD, were measured. As shown in Figure 8C, TRAP activity was dose-dependently reduced, and it was significantly decreased in the cells treated with 20 μ g/mL liposomal CRE-SD. Moreover, F4/80 staining was used to assess the proportion of macrophages in each cell sample. In Figure 8D and Figure A2, there are numerous brown patches in the RAW 264.7 cell samples treated with CRE-SD-FREE-LIP, owing to the high number of macrophages. The rarity of brown patches was apparent in the 20 ng/mL RANKL-stimulated RAW 264.7 cell samples. However, this was reversed in 20 μ g/mL liposomal CRE-SD. This finding was supported by the percentage of F4/80-positively stained cells (Figure 8E), which was reduced after stimulation of CRE-SD-FREE-LIP-treated RAW 264.7 cells with 20 ng/mL RANKL. When 20 μ g/mL liposomal CRE-SD was applied to the RANKL-stimulated RAW 264.7 cells, there was a significant increase in this percentage. Further, RT-PCR was performed to measure the expression of osteoclast markers (CTSK, c-Fos, and NFATc1). After the addition of 10 and 20 μ g/mL liposomal CRE-SD to 20 ng/mL RANKL-stimulated RAW 264.7 cells, the fainter bands of the preceding osteoclast markers developed in a dose-dependent manner (Figure 8F and Figure A3). The expression of c-Fos significantly decreased in the cells treated with 10 μ g/mL liposomal CRE-SD. Significant reductions in the expressions of CTSK, c-Fos, and NFATc1 were found in the cells treated with 20 μ g/mL liposomal CRE-SD (Figure 8G–I).

3.6 Suppressive effect of liposomal CRE-SD on I κ B α /p65 phosphorylation in osteoclastogenesis

Western blotting was utilized to detect the phosphorylation of I κ B α and p65. The Western blot images of p-p65, total p65, p-I κ B α , and total I κ B α proteins in 20 ng/mL RANKL-stimulated RAW 264.7 cells treated with CRE-SD-FREE-LIP and liposomal CRE-SD (10 and 20 μ g/mL) are illustrated in Figure 9A and Figure A4. Significant downregulations of p65 and I κ B α phosphorylation were observed after exposure to liposomal CRE-SD in a dose-dependent manner (Figure 9B,C).

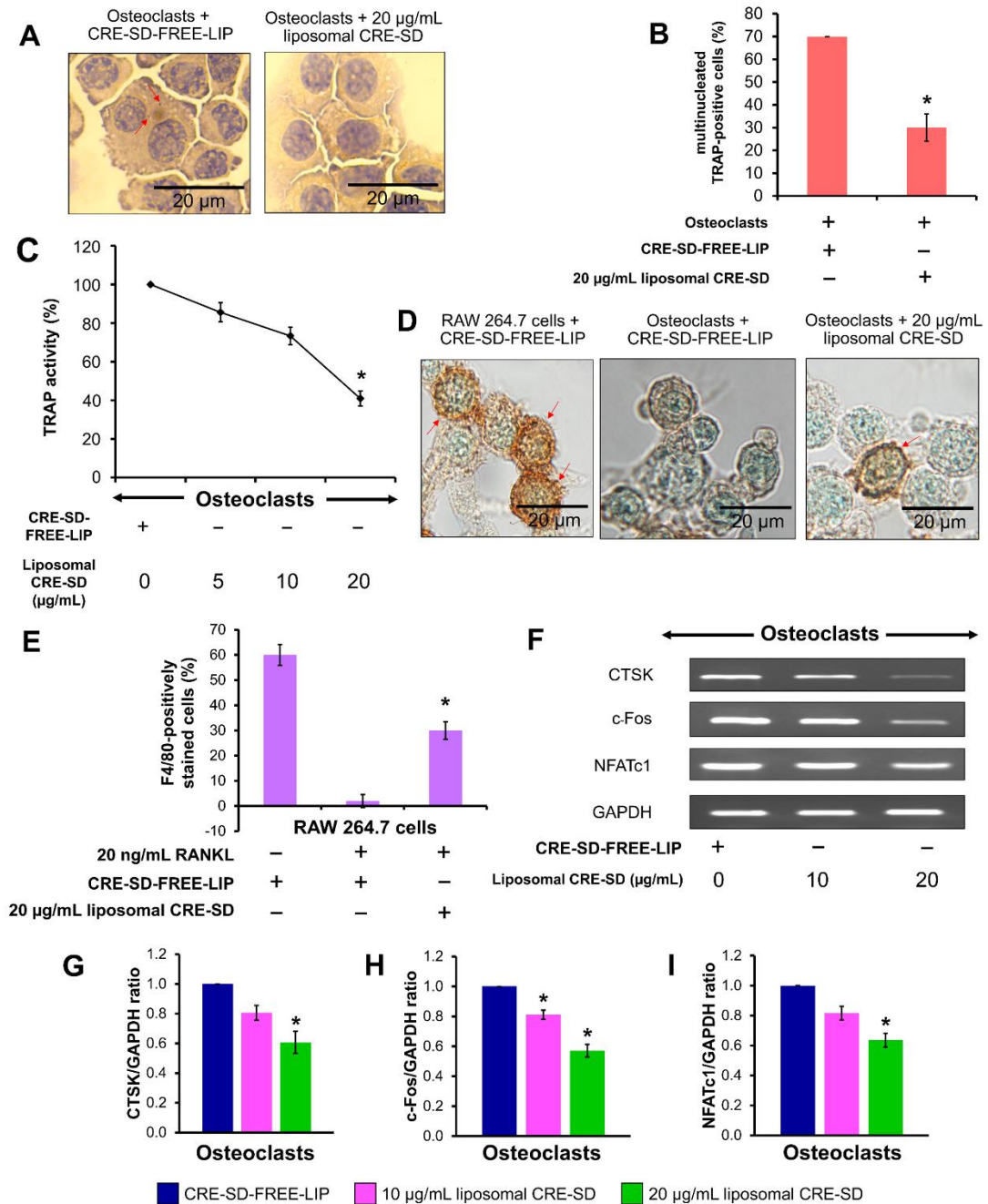


Figure 8 Osteoclastogenic examination

(A) Morphological examination after TRAP staining. First, 20 ng/mL RANKL-stimulated RAW 264.7 cells treated with CRE-SD-free POPC liposomes (CRE-SD-FREE-LIP) and 20 $\mu\text{g}/\text{mL}$ liposomal CRE-SD were stained. The arrows indicate stained granules. (B) Percentage of multinucleated TRAP-positive cells in 20 ng/mL RANKL-stimulated RAW 264.7 cells treated with CRE-SD-FREE-LIP and 20 $\mu\text{g}/\text{mL}$ liposomal CRE-SD. (C) TRAP activity of 20 ng/mL RANKL-stimulated RAW 264.7 cells. The CRE-SD-FREE-LIP and liposomal CRE-SD (5, 10, and 20 $\mu\text{g}/\text{mL}$) were incorporated into the cell samples. (D) Morphological examination after

immunocytochemistry analysis of F4/80 was performed. RANKL-unstimulated RAW 264.7 cells treated with CRE-SD-FREE-LIP and 20 ng/mL RANKL-stimulated RAW 264.7 cells treated with CRE-SD-FREE-LIP and 20 μ g/mL liposomal CRE-SD were examined. Arrows indicate F4/80-positively stained cells. (E) The percentage of F4/80-positively stained cells. RANKL-unstimulated RAW 264.7 cells treated with CRE-SD-FREE-LIP and 20 ng/mL RANKL-stimulated RAW 264.7 cells treated with CRE-SD-FREE-LIP and 20 μ g/mL liposomal CRE-SD were utilized. (F) RT-PCR analysis of osteoclast markers (CTSK, c-Fos, and NFATc1); 20 ng/mL RANKL-stimulated RAW 264.7 cells were treated with CRE-SD-FREE-LIP and liposomal CRE-SD (10 and 20 μ g/mL). (G) CTSK/GAPDH ratio. (H) c-Fos/GAPDH ratio. (I) NFATc1/GAPDH ratio. Statistically significant differences between the corresponding samples and the control are denoted as * $p < 0.05$, $n = 3$.

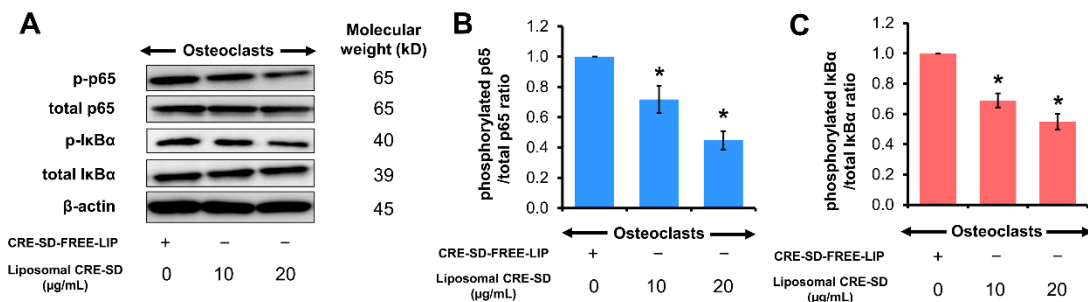


Figure 9 Regulatory effect of liposomal CRE-SD on p65 and I κ B α phosphorylation

(A) Western blots of phosphorylated p65 (p-p65), total p65, phosphorylated I κ B α (p-I κ B α), and total I κ B α after exposure of 20 ng/mL RANKL-stimulated RAW 264.7 cells to liposomal CRE-SD. (B) The p-p65/total p65 ratio after exposure of 20 ng/mL RANKL-stimulated RAW 264.7 cells to liposomal CRE-SD. (C) The p-I κ B α /total I κ B α ratio after 20 ng/mL RANKL-stimulated RAW 264.7 cells were exposed to liposomal CRE-SD. Statistically significant differences between the corresponding liposomal CRE-SD-treated and CRE-SD-FREE-LIP-treated samples are denoted as * $p < 0.05$, $n = 3$.

3.7 Inhibitory effect of liposomal CRE-SD on nuclear translocation and transcriptional activity of p-p65 in osteoclastogenesis

To corroborate the effects of liposomal CRE-SD on nuclear translocation and the transcriptional activity of p-p65, Western blotting analysis was used to examine the p65 phosphorylation of 20 ng/mL RANKL-stimulated RAW 264.7 cells. As shown in Figure 10 and Figure A5, the p-p65/total p65 ratio decreased when 20 ng/mL RANKL-stimulated RAW 264.7 cell samples were treated with 20 μ g/mL liposomal CRE-SD. In contrast, there was a significant reversal after 20 ng/mL RANKL-stimulated RAW 264.7 cell samples were treated with JSH23 and 20 μ g/mL liposomal CRE-SD.

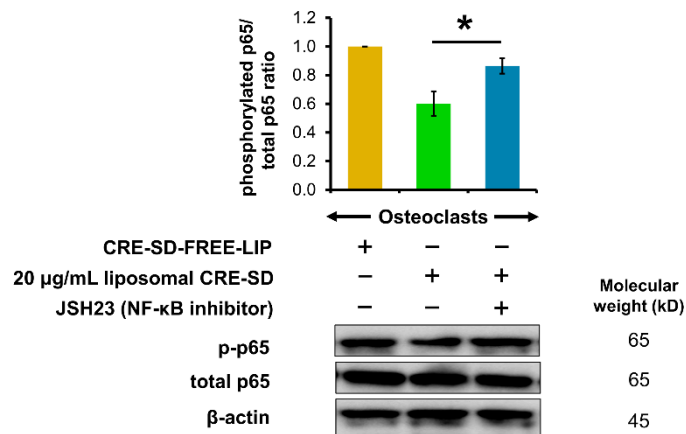


Figure 10 Regulatory effect of liposomal CRE-SD on p65 phosphorylation after incorporating JSH23

The Western blots and p-p65/total p65 ratio after subjecting 20 ng/mL RANKL-stimulated RAW 264.7 cells to 20 µg/mL liposomal CRE-SD and JSH23 are shown. Statistical significance of the difference between the samples treated with 20 µg/mL liposomal CRE-SD and JSH23 and the samples treated with 20 µg/mL liposomal CRE-SD is denoted as * $p < 0.05$, $n = 3$.

3.8 Inhibition of liposomal CRE-SD on intracellular ROS production in osteoclastogenesis

First, 20 ng/mL RANKL-stimulated RAW 264.7 cells were treated with CRE-SD-FREE-LIP and liposomal CRE-SD (5, 10, and 20 µg/mL) to analyze the production of intracellular ROSs. As shown in Figure 11, there was a dose-dependent reduction in the percentage of ROSs produced in the cells. Furthermore, such a proportion significantly decreased in the cells treated with 20 µg/mL liposomal CRE-SD.

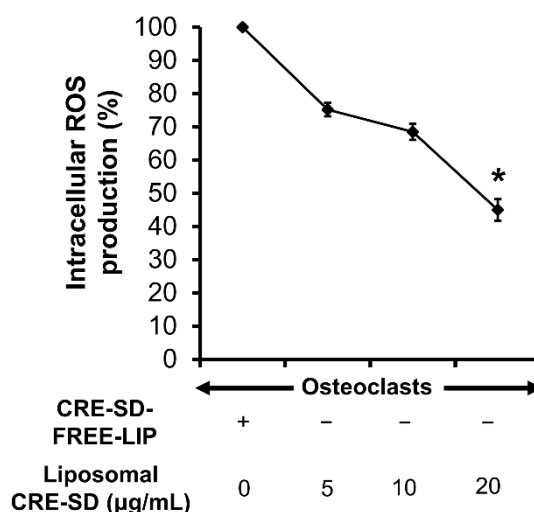


Figure 11 Percentage of intracellular reactive oxygen species (ROSs) produced in 20 ng/mL RANKL-stimulated RAW 264.7 cells

The cells were treated with CRE-SD-FREE-LIP and liposomal CRE-SD (5, 10, and 20 µg/mL). Statistical significance of the difference between the corresponding liposomal CRE-SD-treated and CRE-SD-FREE-LIP-treated samples is denoted as *. $p < 0.05$, $n = 3$.

3.9 Blind docking simulation between IκBα/p50/p65 protein complex and Cu/De/Bis

Following the completion of structure checking and cavity detection processes in CB-Dock2, information on the five largest binding pockets of the IκBα/p50/p65 protein complex was computed using CurPocket (Table 5), along with their possible contact residues (Figure 12A–E and Table 6). After the CB-Dock2 blind docking simulation between the IκBα/p50/p65 protein complex and Cu/De/Bis, the docking result with the greatest negative Vina score was selected to analyze the protein–curcuminoid interactions. The results in Table 7 demonstrate that Cu most probably interacted with binding pocket No.1 (Vina score = -8.0 kcal/mol), whereas De/Bis may have the highest binding affinity to binding pocket No. 2 (Vina score for De = -9.2 kcal/mol; Vina score for Bis = -8.8 kcal/mol). The possible contact residues of these binding pockets are shown in Table 8. There was an abundance of van der Waals forces and classical or conventional hydrogen bonds. Moreover, a moderate number of hydrophobic interactions (π , alkyl, and mixed π /alkyl (e.g., π -sigma and π -alkyl) hydrophobic interactions) were found in the Cu/De/Bis docking results. In Figure 9A–I, some of the intramolecular interactions within the curcuminoids are presented, along with some favorable intermolecular curcuminoid–protein interactions, including classical and non-classical (e.g., carbon and π -donor) hydrogen bonds, electrostatic interactions (e.g., π -charge (π -cation and π -anion) interactions), alkyl and mixed π /alkyl hydrophobic interactions, and π -sulfur interactions.

Table 5 CurPocket-based information on the five largest binding pockets of I κ B α /p50/p65 protein complex

Binding pocket	Cavity volume (\AA^3)	Center (x, y, z)	Cavity size (x, y, z)
1	5316	21.2, 32.5, 4.8	30, 30, 30
2	2633	49.8, 32.5, 31.0	21, 22, 29
3	1341	28.0, 30.0, 26.4	15, 20, 17
4	1291	44.2, 16.7, 44.0	21, 15, 24
5	654	42.0, 25.7, 49.6	18, 16, 14

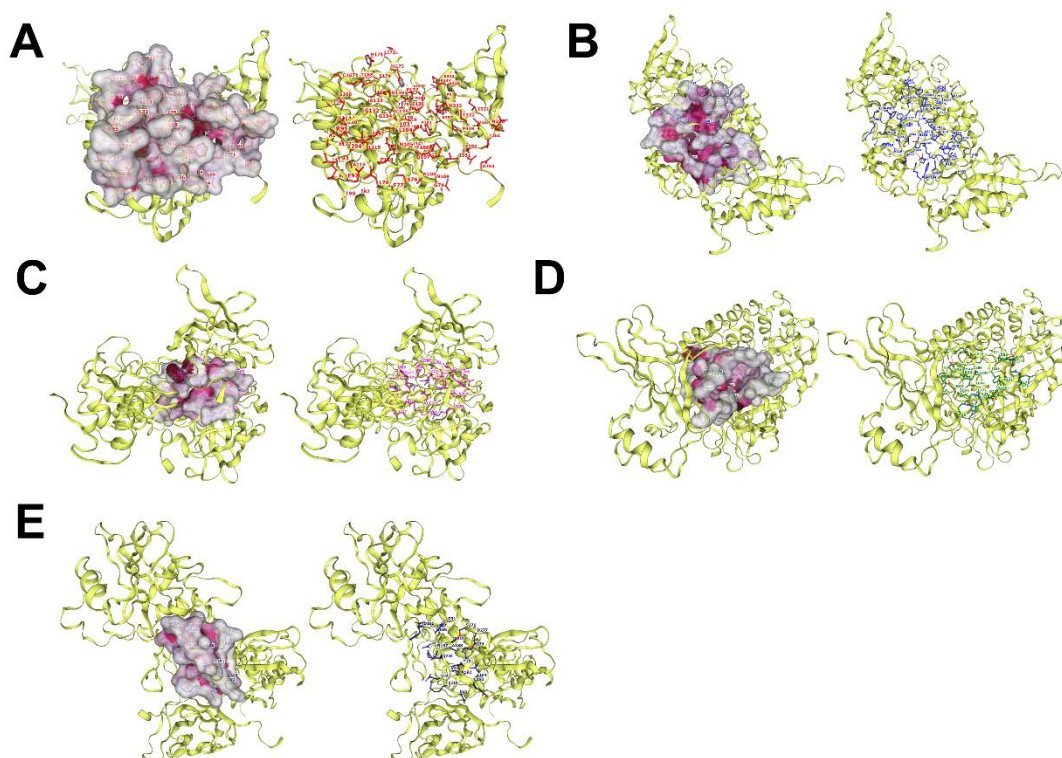


Figure 12 The 3D structures of five predicted binding pockets of I κ B α /p50/p65 protein complex derived from CurPocket

(A) Binding pocket 1. (B) Binding pocket 2. (C) Binding pocket 3. (D) Binding pocket 4. (E) Binding pocket 5.

Table 6 Possible contact residues of five predicted binding pockets of I κ B α /p50/p65 protein complex derived from CurPocket

Binding pocket	Possible contact residues
1	<p>Chain C</p> <p>(SER326, LEU346, PRO344, THR256, PHE345, PRO324, ASN320, LYS343, THR261, VAL319, ASP353, ILE351, ALA257, VAL260, ILE321, LYS323, PRO349, GLU350, THR322)</p> <p>Chain D</p> <p>(GLY134, ASN105, CYS135, PHE103, GLY132, SER174, THR90, LEU78, TYR248, VAL93, HSD171, GLN111, ASN109, ARG140, LEU172, ILE175, LEU139, PHE77, THR179, PHE106, LEU130, LEU131, LEU115, GLY183, ASP136, ALA133, HSD173, ALA118, ASN108, MET91, ILE82, SER76, CYS167, ALA127, THR164, TYR181, THR169, THR168, SER166, PRO147, ILE126, LEU163, ILE94, GLU92, ARG95, ASP141, LEU104, GLN107, GLU138, GLY74, PRO137, ALA129, PRO114, ASN180, PRO214, THR113)</p>
2	<p>Chain A</p> <p>(GLN29, LYS79, HSD181, HSD245, ARG158, GLU222, HSD83, ALA242, VAL248, ARG30, VAL244, ASP80, PRO182, ARG246, LYS221, VAL219, GLN247, GLN220, PHE184, PRO81, GLN241, LYS218)</p> <p>Chain C</p> <p>(ARG305, ASN247, VAL251, ASP271, LYS249, GLN306, PHE307)</p> <p>Chain D</p> <p>(THR247, TYR248, TYR289, ASP290, SER293, GLN212, MET279, SER283, GLU286, GLU287, GLU282, VAL246, GLY217, ARG245, SER288, TYR251, GLY250, PRO281, THR291, LEU280, GLN249, GLU292, TRP258)</p>

Binding pocket	Possible contact residues
3	Chain A (ARG253, ARG201, GLU211, ASN200, PHE213) Chain C (THR256, ARG252, ARG255, ILE266, ALA257, GLU264, GLU265, TYR267, ASP254) Chain D (CYS215, TYR181, ILE192, ASN216, GLU213, ARG218, LEU223, HSD184, LEU227, ASP226, ASN182)
4	Chain A (ARG273, GLN26, ASP53, GLN29, HSD181, SER276, ARG236, SER51, LYS28, GLU222, GLU225, VAL244, GLY44, ARG30, ARG33, ARG35, ARG278, GLY237, ARG50, LYS221, MET32, ILE224, PRO47, SER45, PHE239, SER42, ALA43, PRO27, THR52, SER238, GLU49, PRO275, ASP223, GLY31, SER240, GLN241) Chain D (ARG260, GLN266, GLY259, TRP258)
5	Chain A (ASN186, ASP217, ARG274, ALA192, PHE184, ALA188, ARG187, VAL219, THR191, GLN247, LEU194, ASP185, SER276, ASP223, ARG30, GLN220, GLY31, ASP277, GLU193, LYS218)

Table 7 The I κ B α /p50/p65 binding pockets with the greatest negative Vina scores after blind docking with curcuminoids

Ligand	Binding pocket	Vina score (kcal/mol)	Cavity volume (Å ³)	Docking center (x, y, z)	Docking size (x, y, z)
Curcumin	1	-8.0	5316	21, 33, 5	35, 35, 35
Demethoxycurcumin	2	-9.2	2633	50, 33, 31	27, 27, 34
Bisdemethoxycurcumin	2	-8.8	2633	50, 33, 31	26, 26, 34

Table 8 Possible contact residues of the I κ B α /p50/p65 binding pockets in Table 7

Ligand	Contact residues
Curcumin	Chain C: THR256 ALA257 PRO324 PRO344 PHE345 LEU346 Chain D: GLU138 ARG140 GLY144 HIS173 LYS177 ALA178 THR179 ASN180 TYR181 ASN182 GLY183 THR185 GLN212 PRO214
Demethoxycurcumin	Chain A: GLN29 ARG30 LYS79 HIS181 PRO182 PHE184 VAL219 GLN220 LYS221 GLU222 GLN241 VAL244 HIS245 ARG246 GLN247 Chain D: TYR251 TRP258 MET279 LEU280 PRO281 GLU282 SER283 GLU287 SER288
Bisdemethoxycurcumin	Chain A: LYS221 GLU222 VAL244 HIS245 ARG246 GLN247 Chain C: ASN247 LYS249 VAL251 ASP271 Chain D: TYR248 GLN249 GLY250 TYR251 PRO281 GLU282 SER283 GLU284 GLU287 SER288 TYR289 ASP290 THR291 GLU292 SER293

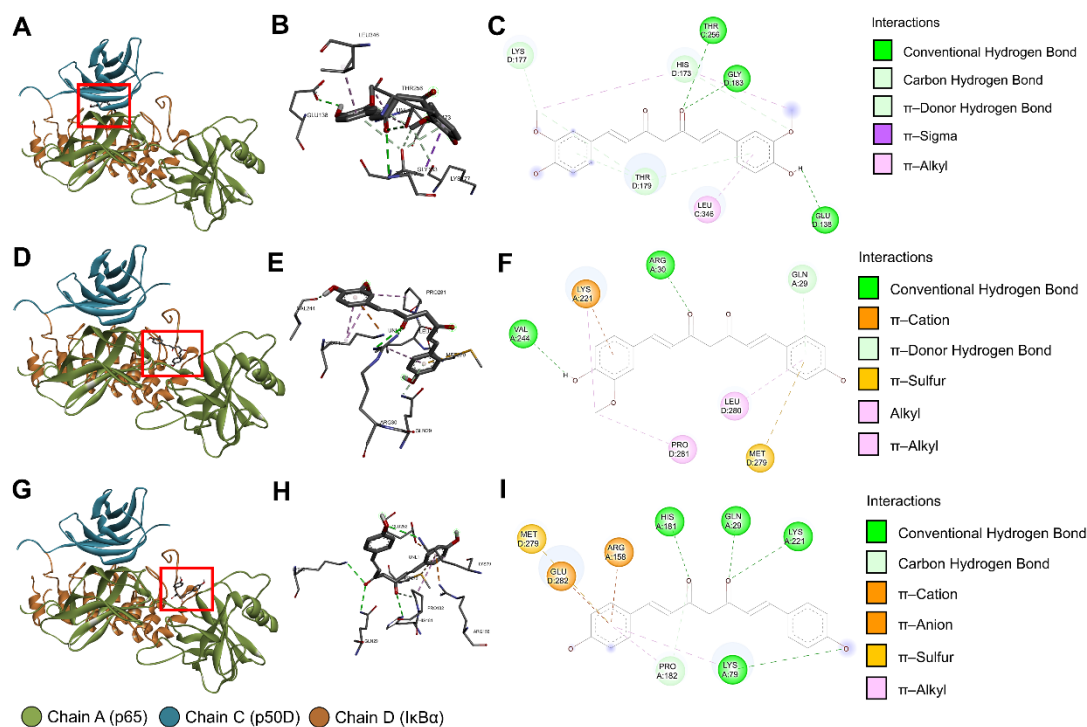


Figure 13 CB-Dock2 blind docking results of the I κ B α /p50/p65 protein complex and curcumin/demethoxycurcumin/bisdemethoxycurcumin

(A) The three-dimensional (3D) binding pose of curcumin. (B) The 3D interactions between the I κ B α /p50/p65 protein complex and curcumin. (C) The two-dimensional (2D) diagram of the interactions between the I κ B α /p50/p65 protein complex and curcumin. (D) The 3D binding pose of demethoxycurcumin. (E) The 3D interactions between the I κ B α /p50/p65 protein complex and demethoxycurcumin. (F) The 2D diagram of the interactions between the I κ B α /p50/p65 protein complex and demethoxycurcumin. (G) The 3D binding pose of bisdemethoxycurcumin. (H) The 3D interactions between the I κ B α /p50/p65 protein complex and bisdemethoxycurcumin. (I) The 2D diagram of the interactions between the I κ B α /p50/p65 protein complex and bisdemethoxycurcumin. The red rectangles indicate the locations of the curcuminoid molecules, and the light green spheres in the 3D interactions indicate intramolecular interactions within the curcuminoid molecules. In the 2D diagrams and 3D interactions, the colored dashed lines linking the protein complex and curcuminoid denote favorable intermolecular interactions. The three-letter amino acid codes and positions of the contact residues are shown in the 3D interactions. The colored circles in the 2D diagrams denote the three-letter amino acid codes, occupying protein chains, and amino acid positions of the contact residues. The light blue circles surrounding the preceding circles are solvent-accessible surfaces. All figures were constructed using BIOVIA discovery studio visualizer.

3.10 The Inhibitory Effect of Liposomal CRE-SD on Osteoclastogenesis via the Canonical NF- κ B Signaling Pathway

The *in vitro* modulatory effect of liposomal CRE-SD on osteoclast differentiation through the canonical NF- κ B signaling pathway is shown in Figure 14. Illustrating this, liposomal CRE-SD reduced p65 and I κ B α phosphorylation, as well as the nuclear translocation and transcriptional activity of p-p65 initiated by the RANK-RANKL interaction. Eventually, osteoclastogenesis was suppressed, as substantiated by the lower number of osteoclasts and decreased expression of osteoclast markers (TRAP, CTSK, c-Fos, and NFATc1), together with a higher expression of F4/80 in undifferentiated murine RAW 264.7 cells.

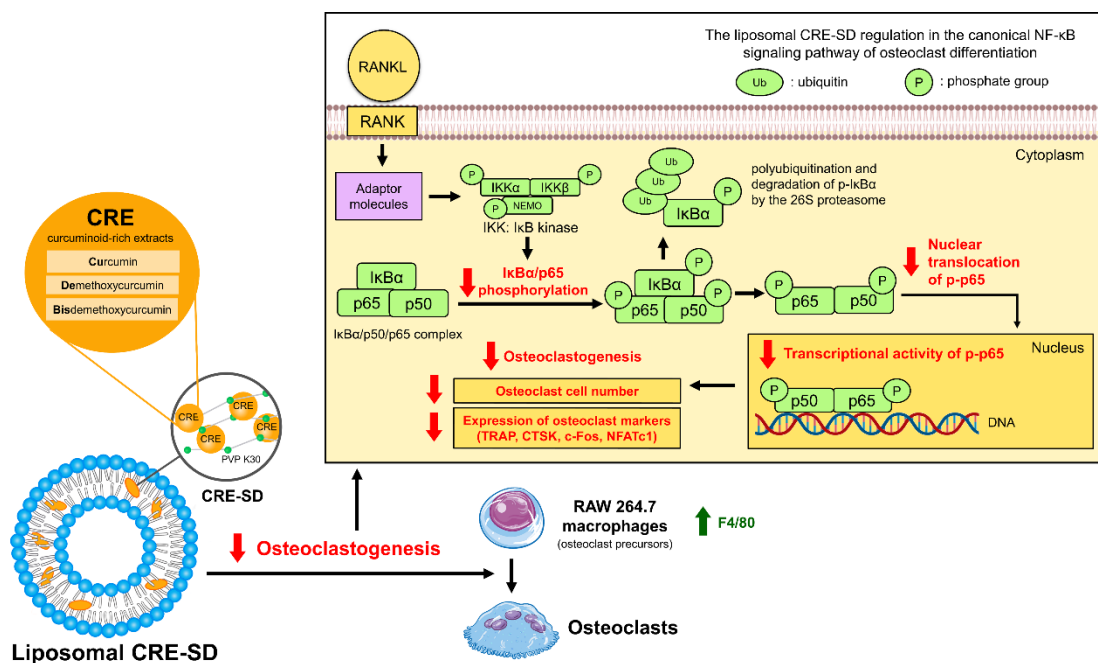


Figure 14 The inhibitory effect of liposomal CRE-SD on osteoclastogenesis via the canonical NF- κ B signaling pathway

CHAPTER 4

DISCUSSION

Numerous drug formulations have been developed in an effort to improve the bioavailability of Cu, De, and Bis. Many clinical trials have shown that most curcuminoid formulations are safe and exhibit well-tolerated properties and excellent therapeutic efficacy with no serious adverse side effects; however, some curcuminoid formulations have been reported to exert side effects. For example, leukopenia, nausea, fatigue, and diarrhea after the administration of curcumin phosphatidylcholine and irinotecan in patients with solid tumors; anemia and hemolysis after the application of the liposomal curcumin Lipocurc™ in patients with locally advanced or metastatic tumors; and mild gastrointestinal symptoms in patients with Parkinson's disease treated with curcumin nanomicelles have all been reported [74]. Regarding bone diseases, various curcuminoid formulations have been developed to treat osteoporosis, osteoarthritis, and RA. The oral administration of 110 mg/day curcumin with 5 mg/day alendronate prevented osteoporosis in 60 postmenopausal women by decreasing the levels of bone-specific alkaline phosphatase and C-terminal cross-linking telopeptides of type I collagen, as well as increasing the levels of osteocalcin and bone mineral density. The combined treatment could also minimize the side effects of alendronate [75,76]. The pharmaceutical advantages of safety, tolerability, and efficacy of diverse curcuminoid formulations have been demonstrated in patients with osteoarthritis [75]. The curcuminoid–turmeric matrix formulation (containing 50% total curcuminoids (41.2% Cu, 7.3% De, and 1.5% Bis), 3% essential oils, 2% protein, and 40% total carbohydrates) reduced the levels of C-reactive protein and rheumatoid factor, as well as the rate of erythrocyte sedimentation, and lowered disease activity scores/indexes in patients with RA, with no serious adverse side effects [74,75]. Owing to the above-mentioned pharmacological advantages, the development of novel curcuminoid formulations may facilitate the effective treatment of bone diseases. However, it is necessary to understand their biological effects by performing *in vitro* experiments and *in silico* analyses.

In this study, the biochemical regulation of liposomal CRE-SD in osteoclastogenesis via the canonical NF- κ B pathway was clarified using both *in vitro* and *in silico* analyses. Liposomal characterization revealed that the liposome diameter was larger when CRE-SD was encapsulated in the POPC liposomes, similar to previous work showing that the solubilization of curcumin in the POPC bilayer of a liposome suspension may contribute to an increase in liposome size [52]. Several reports have mentioned the acceptable values of PDI and zeta potential to ensure that the liposome system is stable. The acceptable PDI, which is between 0 and 0.3, results in a narrow liposome size distribution and a low probability of liposome aggregate formation. An acceptable zeta potential (beyond ± 30 mV) indicates the high stability of the liposome system, on account of electrostatic activity and steric effects [77-79]. Here, the PDI of the liposomal CRE-SD was comparable with that of the CRE-SD-FREE-LIP. Both

values are approximately the PDI of POPC liposome suspensions with and without CRE-Ter (the ternary complex of CRE prepared by dispersing PVP K30 (9% w/w) to the CRE, incorporating HPBCD (molar ratio = 1:1) to the CRE and performing solvent evaporation under reduced pressure, respectively; CRE-Ter contains 14% w/w curcuminoids, as demonstrated in the work of Pengjam et al. [60]. The zeta potentials, at pH 7.4, of both CRE-SD-treated and CRE-SD-FREE-LIP samples were negative, owing to the negatively charged POPC component of the liposomes. Moreover, there was a decrease in the zeta potential after treating CRE-SD in the liposome suspension. The change in such a value may be caused by the partial deprotonation of Cu/De/Bis in CRE-SD at pH 7.4 in PBS, i.e., the partial deprotonated form of the curcuminoids may provide negatively charged ions, therefore reducing the zeta potential [80]. Although the zeta potential of the liposomal CRE-SD samples met the criterion previously mentioned, the PDI may be a shortcoming that could lead to liposome aggregation. Additionally, regarding the review of Takechi-Haraya et al., the liposomal CRE-SD and CRE-SD-FREE-LIP applied in this study are polydisperse, owing to the PDI > 0.4 measured using a DLS instrument [81]. Further microscopic examination, such as through a transmission electron microscope (TEM), to assess the size distribution of liposomes with the PDI derived from DLS instrument > 0.4 was suggested by Takechi-Haraya et al. [81]. Nevertheless, conducting this microscopic observation in this study was constrained by the unavailability of electron microscopy resources. Wahyudiono et al. reported that the injection of a greater concentration of phospholipids, comprising POPC, into a medium brings about an enhancement in liposome size and PDI [82]. Previous studies by Csicsák et al. and Lee mentioned that the reduction in the size of drug particles can increase their surface area, resulting in an improvement in their dissolution and bioavailability, along with a narrow size distribution for drug particles [83-84]. In other words, decreasing the concentration of POPC utilized to produce liposomal CRE-SD may lead to reduced liposome size and PDI, as well as enhanced bioavailability. Thus, further research is needed to optimize the amount of POPC required to encapsulate the CRE-SD into liposomes, particularly before testing the pharmaceutical effectiveness of liposomal CRE-SD in *in vivo* studies and clinical trials.

Paradkar et al. analyzed the scanning electron microscope (SEM) images of curcumin–PVP K30 solid dispersions prepared through spray drying. The images showed spherical particles in curcumin/PVP K30 samples. The particles of the samples with higher proportions of PVP K30 (curcumin/PVP K30 ratios of 1:5–1:10) had smoother surfaces than those with curcumin/PVP K30 ratios of 1:1–1:3. Additionally, the surface of the former had concave depressions [85]. Considering the SEM images of Chhouk et al. [86], the particle sizes of PVP microspheres containing curcumin prepared via electrospraying was smaller than those of unmodified PVP particles. The incorporation of curcumin with PVP can increase conductivity and reduce particle size [86]. Machmudah et al. mentioned that modifying the surfaces of solutes with hydrophilic polymer carriers, in which PVP K30 is included, as well as decreasing the size of solutes, can increase the solubility. The former can also prevent the agglomeration of the particle product. Furthermore, the intermolecular interaction

between curcumin and PVP can lead to a higher thermal stability of curcumin via carboxyl and carbonyl conjugations [87]. Altogether, the addition of PVP to curcumin may improve the solubility and stability of curcumin, resulting in better pharmacokinetic properties. Although SEM images and analytical chemistry experiments can provide more information on the morphological and chemical characteristics of the CRE-SD, which may affect its pharmacokinetic attributes, the resources of SEM and analytical chemistry instruments were unavailable in this study. Hence, further research is needed to analyze such CRE-SD characteristics.

Laouini et al. conducted TEM observation and a stability study to examine some characteristics of POPC liposomes. The micrograph showed that such liposomes were spherical. Throughout the storage period (3 months; stored at 5 ± 3 °C), there was low variation in their average size and zeta potential. In addition, neither aggregation nor sedimentation was found [88]. The *in vitro* examination of CRE-SD release in this study identified a lower percentage of the cumulative mass of CRE-SD lost from the dialysis sac of liposomal CRE-SD samples over 70 days, in comparison with that lost from CRE-SD samples. The slight change in this percentage from the liposomal CRE-SD samples over 70 days indicated the highly controlled and sustained release of the CRE-SD encapsulated in the POPC liposomes. Thus, utilizing POPC liposome encapsulation in the CRE-SD may lead to higher stability with a long shelf-life (70 days) compared with CRE-SD. Compared to the 60-day *in vitro* assessment of liposomal CRE-Ter release performed by Pengjam et al., as well as the analysis of a Cu-loaded DMPC liposomes/3D-printed tricalcium phosphate (TCP) scaffold conducted by Sarkar and Bose, the proportion of CRE-SD in the liposomal CRE-SD samples developed in this study decreased by approximately 5–10% and approximately 5–12%, respectively [53,60]. Consequently, this implies that liposome encapsulation can improve the pharmacokinetic properties of CRE-SD, and those of liposomal CRE-SD may be superior to the liposomal CRE-Ter and Cu-loaded DMPC liposomes/3D-printed TCP scaffold. However, further *in vivo* and clinical studies exploring the safety and efficacy of liposomal CRE-SD are required to confirm the pharmacological practicality of liposomal CRE-SD.

Although some properties of liposomal CRE-SD and the *in vitro* release of CRE-SD were investigated in this study, the interaction between CRE-SD and the POPC bilayers of the liposomes remains unexplored. Currently, the interactions between curcumin and POPC lipid bilayers have been illustrated. Ercan [89] used coarse-grained molecular dynamics to analyze the interactions between curcumin and lipid bilayers composed of regular POPC (containing one unsaturated chain), and those composed of regular DOPC (1,2-dioleoyl-sn-glycero-3-phosphocholine; containing two unsaturated chains) with different curcumin/lipid molar ratios. The calculated membrane thickness of regular POPC lipids was greater than that of regular DOPC lipids, in contrast to the area per lipid headgroup. Furthermore, introducing a higher amount of curcumin led to lower membrane thickness and a greater area per lipid headgroup in both regular POPC and DOPC lipids. The changes in the membrane thickness and area per lipid headgroup may be caused by the changes in the binding

orientation and binding states of curcumin [89]. As the lipid compositions and the concentration of curcumin alter the size of the bilayer membrane, these factors may affect the bioavailability of curcumin. Hence, further elucidation of the interactions between CRE-SD and POPC bilayers, as well as the changes in the related parameters of POPC, is warranted to understand the effect of liposomal CRE-SD formation on its bioavailability.

The RANKL incubation time and liposomal CRE-SD concentration were optimized. Following CRE-SD-FREE-LIP and 20 ng/mL RANKL treatments for up to 5 days, the TRAP activity and the relative expression of CTSK in the RAW 264.7 cells were significantly increased on days 3–5 and days 4–5, respectively, indicating a tendency toward osteoclastogenesis within these periods. This finding can be determined that the optimal incubation time for liposomal-treated RANKL-stimulated RAW 264.7 cells should be at least 4 days. However, in further *in vitro* experiments, a 5-day incubation period after treatment with CRE-SD-FREE-LIP, liposomal CRE-SD, and/or RANKL was applied for RAW 264.7 cells, as previous reports described the attainment of osteoclastogenic stimulation using a 5-day incubation period in liposomal-treated and liposomal-untreated RANKL-stimulated RAW 264.7 cell samples [4,55]. The cell viability in 20 ng/mL RANKL-stimulated RAW 264.7 cells treated with various concentrations of liposomal CRE-SD was assessed to determine the maximum dose of liposomal CRE-SD that did not give rise to cytotoxicity, as indicated by a significant depletion in the number of viable cells. A significant reduction in viable cell number was found in 20 ng/mL RANKL-stimulated RAW 264.7 cells treated with 30 $\mu\text{g}/\text{mL}$ liposomal CRE-SD. Therefore, the highest concentration of liposomal CRE-SD that did not induce cytotoxicity was 20 $\mu\text{g}/\text{mL}$, which was applied for the subsequent *in vitro* analyses.

Then, morphological examinations were conducted, and osteoclast marker expression was measured. The TRAP staining, TRAP assay, and RT-PCR results confirmed that 20 $\mu\text{g}/\text{mL}$ liposomal CRE-SD may significantly suppress the proportion of osteoclasts (justified by that of multinucleated TRAP-positive cells) and significantly reduce the expressions of osteoclast markers (TRAP, CTSK, c-Fos, and NFATc1) in 20 ng/mL RANKL-stimulated RAW 264.7 cells. In other words, liposomal CRE-SD may hinder osteoclastogenesis. For the immunocytochemistry of F4/80, there were fewer brown patches and a lower percentage of F4/80-positively stained cells after CRE-SD-FREE-LIP-treated RAW 264.7 cells were subjected to 20 ng/mL RANKL. Their inversion was shown in RANKL-stimulated RAW 264.7 cells treated with 20 $\mu\text{g}/\text{mL}$ liposomal CRE-SD. These results suggest a decrease in the proportion of murine macrophages that may be murine RAW 264.7 cells, as RANKL treatment contributes to osteoclastogenesis. In contrast, treating RANKL-stimulated RAW 264.7 cells with 20 $\mu\text{g}/\text{mL}$ liposomal CRE-SD may inhibit osteoclastogenesis, as demonstrated by an increase in the proportion of undifferentiated murine RAW 264.7 macrophages. To put it simply, the immunocytochemistry analysis of F4/80 corroborates the inhibitory effect of liposomal CRE-SD on osteoclastogenesis.

Considering Western blotting, the blot images and the phosphorylated protein/total protein ratios indicated that liposomal CRE-SD may dose-dependently impede the phosphorylation of p65 and I κ B α in 20 ng/mL RANKL-stimulated RAW 264.7 cells. Moreover, these results indicated that the incorporation of JSH23, and subsequent treatment with 20 μ g/mL liposomal CRE-SD, could counteract the suppressed p-p65 expression in 20 ng/mL RANKL-stimulated RAW 264.7 cells. Accordingly, the findings suggest that liposomal CRE-SD can prevent the phosphorylation of p65 and I κ B α , along with the nuclear translocation and transcriptional activity of p-p65 in RANKL-stimulated RAW 264.7 cells.

Previous studies have revealed that ROSs can upregulate NF- κ B transcription factors, resulting in osteoclastogenesis [63,64]. Moreover, curcuminoids have an antioxidant effect, causing the removal of free radicals [65]. The findings revealed a dose-dependent decrease in the production of intracellular ROSs after the incorporation of liposomal CRE-SD into 20 ng/mL RANKL-stimulated RAW 264.7 cells. Hence, it can be inferred that liposomal CRE-SD suppresses ROS production within osteoclasts and, hence, the cellular canonical NF- κ B pathway, resulting in the inhibition of osteoclastogenesis.

Several studies have highlighted the design of liposomal curcuminoids for inhibiting *in vitro* osteoclast differentiation. Yeh et al. showed that Cu- and Bis-loaded soybean phosphatidylcholine (SPC) liposomes hamper osteoclastogenesis [55]. Pengjam et al. typified the impediment of liposomal CRE-Ter in osteoclast differentiation via the NF- κ B and ERK signaling pathways [60], through which its anti-osteoclastogenic regulation through the former supports the *in vitro* findings in this study. Owing to the *in vitro* modulatory effect of liposomal CRE-SD on osteoclast differentiation through the canonical NF- κ B signaling pathway, the liposomal CRE-SD designed in this study may be an alternative herbal medicine for preventing immoderate osteoclast differentiation. Nevertheless, to completely elucidate how liposomal CRE-SD affects the coupling of bone formation and bone resorption, future research should examine the *in vitro* biochemical function of liposomal CRE-SD during osteoblast differentiation. Furthermore, *in vivo* studies and clinical trials are required to confirm the potential of liposomal CRE-SD for the treatment of bone diseases.

In terms of the blind molecular docking simulation, the CB-Dock2 was implemented to investigate the interactions between the I κ B α /p50/p65 protein complex and Cu/De/Bis. The AutoDock Vina algorithm in CB-Dock2 uses the Vina scoring function to calculate the Vina score (unit: kcal/mol), which signifies the curcumin-protein binding energy. A lower (more negative) Vina score designates higher binding affinity [90]. The molecular docking results in this study revealed low Vina scores in the binding between Cu/De/Bis and the I κ B α /p50/p65 protein complex, i.e., the curcuminoids had a strong binding affinity to the protein complex. This can be attributed to high proportions of van der Waals forces, conventional hydrogen bonds, and hydrophobic interactions in the curcuminoid-protein docking mechanism, together with other minor intermolecular interactions. These implications on binding affinity are

supported by a report by Saeed et al. demonstrating the low binding energies of the docking between Cu/De/Bis and the p50/p65 heterodimer complexed to I κ B DNA (PDB ID: 1VKX), computed using the AutoDock program version 4.2.6 [35].

In this study, the 3D curcuminoid–protein docking models and two-dimensional (2D) diagrams of the curcuminoid–protein interactions illustrated numerous favorable intermolecular interactions between Cu/De/Bis and the I κ B α subunit of the protein complex. This might substantiate that these interactions bring about the inhibitory effects of curcuminoids in liposomal CRE-SD on I κ B α phosphorylation, proven in the *in vitro* experiments of this study. Considering the p65-p50 dimer in the protein complex (PDB ID: 1IKN), the N-terminal RHR or RHD (positions 19–315 of p65 and positions 39–368 of p50) consists of functional sequences, i.e., a DNA-binding subdomain (positions 19–185 of p65 and positions 39–238 of p50), a dimerization subdomain (positions 191–291 of p65 and positions 245–350 of p50), and a NLS (positions 301–304 of p65 and positions 361–363 and 365 of p50) [27]. Many of the favorable intermolecular interactions shown in the docking output of this study indicated the binding of the curcuminoids to such functional sequences. Cu binds to the dimerization subdomain of p50 at THR256 via conventional hydrogen bonding, and at LEU346 via π –alkyl interactions. De binds to the DNA-binding subdomain of p65 at GLN29 via π –donor hydrogen bonds, and at ARG30 via conventional hydrogen bonding. It also binds to the dimerization subdomain of p65 at LYS221 via alkyl, π –alkyl, π –donor, and π –cation interactions, and at VAL244 via conventional hydrogen bonding. Bis binds to the DNA-binding subdomain of p65 at GLN29, LYS79, and HIS181 via conventional hydrogen bonding, at ARG158 via π –cation interaction, and at PRO182 via carbon–hydrogen bonds and π –alkyl interactions. Furthermore, it binds to the dimerization subdomain of p65 at LYS221 via conventional hydrogen bonding. These findings suggest that the interactions of the curcuminoids in liposomal CRE-SD to DNA binding and dimerization subdomains may cause an impediment of p65-p50 dimerization and the binding of the p65-p50 dimer to nuclear DNA. The CB-Dock2 docking revealed that there were no interactions between the curcuminoids and the NLS of the p65 and p50 subunits, contradicting the AutoDock version 4.0 docking simulation results of curcumin, as reported by Cheemanapalli et al. [34]. A plausible cause for this is a difference in the binding pocket prediction methods. The CurPocket in CB-Dock2 retrieves the binding pocket candidates by screening the clusters of concave surfaces, whereas the CASTp program, which Cheemanapalli et al. utilized for identifying protein active sites, creates the binding pocket profile using the alpha shape method [34,73,91,92]. In this study, owing to the absence of the NLS residues in the top-five binding pocket information derived from the CurPocket cavity detection process, the NLS residues were not implemented in CB-Dock2 blind docking. The *in vitro* experiments by Riedlinger et al. mentioned that monomeric p65 can be rapidly degraded and ineffectively translocated to the nucleus [93]. For this reason, the *in silico* findings in this study implied that the suppression of p65-p50 dimerization and the binding between p65 and DNA arising from the curcuminoid intermolecular interactions may reduce the stability of p65 and, consequently, inhibit its

phosphorylation, nuclear translocation, and DNA binding. Although this inference corroborates the *in vitro* results, it cannot fully confirm the hindrance of liposomal CRE-SD on the canonical NF- κ B signaling pathway during osteoclastogenesis, owing to the lack of Western blotting data concerning the regulatory effect of liposomal CRE-SD on p50 phosphorylation.

CHAPTER 5

CONCLUSION

In summary, liposomal encapsulation and PVP K30 solid dispersion to a CRE containing Cu, De, and Bis were applied to acquire liposomal CRE-SD. The *in vitro* experiments corroborated the potential of liposomal CRE-SD to inhibit osteoclastogenesis (the differentiation of RANKL-stimulated murine RAW 264.7 macrophages) via the canonical NF- κ B signaling pathway. Furthermore, the molecular docking simulation demonstrated that the intermolecular interactions between the curcuminoids in liposomal CRE-SD and the I κ B α /p50/p65 protein complex may contribute to such suppressive regulation. These findings manifested that liposomal CRE-SD is a promising herbal candidate for bone disease treatment; nevertheless, clarification of its pharmacological effects on osteoblasts, animal models, and patients with bone disease is needed.

BIBLIOGRAPHY

1. Holliday LS, Patel SS, Rody WJ, Jr. RANKL and RANK in extracellular vesicles: surprising new players in bone remodeling. *Extracell Vesicles Circ Nucl Acids*. 2021;2:18-28.
2. Salhotra A, Shah HN, Levi B, Longaker MT. Mechanisms of bone development and repair. *Nat Rev Mol Cell Biol*. 2020;21:696-711.
3. Zhao W, Huang Z, Lin Y, Lan J, Gao X. Inhibition effect of zoledronate on the osteoclast differentiation of RAW264.7 induced by titanium particles. *BioMed Res Int*. 2021;2021:1-7.
4. Cheng Y, Liu H, Li J, Ma Y, Song C, Wang Y, et al. Evaluation of culture conditions for osteoclastogenesis in RAW264.7 cells. *PLoS One*. 2022;17:e0277871.
5. Yao Y, Cai X, Ren F, Ye Y, Wang F, Zheng C, et al. The macrophage-osteoclast axis in osteoimmunity and osteo-related diseases. *Front Immunol*. 2021;12:664871.
6. Al-Bari AA, Al Mamun A. Current advances in regulation of bone homeostasis. *FASEB Bioadv*. 2020;2:668-79.
7. Jiménez JA, Lawlor ER, Lyssiotis CA. Amino acid metabolism in primary bone sarcomas. *Front Oncol*. 2022;12:1001318.
8. Hauser B, Raterman H, Ralston SH, Lems WF. The effect of anti-rheumatic drugs on the skeleton. *Calcif Tissue Int*. 2022;111:445-56.
9. Lu J, Hu D, Ma C, Shuai B. Advances in our understanding of the mechanism of action of drugs (including traditional Chinese medicines) for the intervention and treatment of osteoporosis. *Front Pharmacol*. 2022;13:938447.
10. Oh K-K, Adnan M, Cho D-H. Drug investigation to dampen the comorbidity of rheumatoid arthritis and osteoporosis via molecular docking test. *Curr Issues Mol Biol*. 2022;44:1046-61.
11. Xue S-T, Wang Y-L, Han X-W, Yi H, Jiang W, Si S-Y, et al. Novel cathepsin K inhibitors block osteoclasts *in vitro* and increase spinal bone density in zebrafish. *RSC Adv*. 2019;9:8600-7.

12. LeBoff MS, Greenspan SL, Insogna KL, Lewiecki EM, Saag KG, Singer AJ, et al. The clinician's guide to prevention and treatment of osteoporosis. *Osteoporos Int.* 2022;33:2049-102.
13. Amalraj A, Pius A, Gopi S, Gopi S. Biological activities of curcuminoids, other biomolecules from turmeric and their derivatives – a review. *J Tradit Complement Med.* 2017;7:205-33.
14. Hewlings SJ, Kalman DS. Curcumin: a review of its effects on human health. *Foods.* 2017;6:92.
15. Fuloria S, Mehta J, Chandel A, Sekar M, Rani NNIM, Begum MY, et al. A comprehensive review on the therapeutic potential of *Curcuma longa* Linn. in relation to its major active constituent curcumin. *Front Pharmacol.* 2022;13:820806.
16. Bresciani L, Favari C, Calani L, Francinelli V, Riva A, Petrangolini G, et al. The effect of formulation of curcuminoids on their metabolism by human colonic microbiota. *Molecules.* 2020;25:940.
17. Shen X, Sun X, Chen H, Lu B, Qin Y, Zhang C, et al. Demethoxycucumin protects MDA-MB-231 cells induced bone destruction through JNK and ERK pathways inhibition. *Cancer Chemother Pharmacol.* 2021;87:487-99.
18. Wei J-X, Luo Y, Xu Y, Xiao J-H. Osteoinductive activity of bisdemethoxycurcumin and its synergistic protective effect with human amniotic mesenchymal stem cells against ovariectomy-induced osteoporosis mouse model. *Biomed Pharmacother.* 2022;146:112605.
19. Sivani BM, Azzeh M, Patnaik R, Pantea Stoian A, Rizzo M, Banerjee Y. Reconnoitering the therapeutic role of curcumin in disease prevention and treatment: lessons learnt and future directions. *Metabolites.* 2022;12:639.
20. Huang C, Lu H-F, Chen Y-H, Chen J-C, Chou W-H, Huang H-C. Curcumin, demethoxycurcumin, and bisdemethoxycurcumin induced caspase-dependent and –independent apoptosis via Smad or Akt signaling pathways in HOS cells. *BMC Complement Med Ther.* 2020;20:68.
21. Urošević M, Nikolić L, Gajić I, Nikolić V, Dinić A, Miljković V. Curcumin: biological activities and modern pharmaceutical forms. *Antibiotics (Basel).* 2022;11:135.

22. Racz LZ, Racz CP, Pop L-C, Tomoaia G, Mocanu A, Barbu I, et al. Strategies for improving bioavailability, bioactivity, and physical-chemical behavior of curcumin. *Molecules*. 2022;27:6854.
23. Song JG, Noh H-M, Lee SH, Han H-K. Lipid/clay-based solid dispersion formulation for improving the oral bioavailability of curcumin. *Pharmaceutics* 2022;14:2269.
24. Song J-W, Liu Y-S, Guo Y-R, Zhong W-X, Guo Y-P, Guo L. Nano-liposomes double loaded with curcumin and tetrandrine: preparation, characterization, hepatotoxicity and anti-tumor effects. *Int J Mol Sci*. 2022;23:6858.
25. Capece D, Verzella D, Flati I, Arboretto P, Cornice J, Franzoso G. NF- κ B: blending metabolism, immunity, and inflammation. *Trends Immunol*. 2022;43:757-75.
26. Liu P, Li Y, Wang W, Bai Y, Jia H, Yuan Z, et al. Role and mechanisms of the NF- κ B signaling pathway in various developmental processes. *Biomed Pharmacother*. 2022;153:113513.
27. Florio TJ, Lokareddy RK, Yeggoni DP, Sankhala RS, Ott CA, Gillilan RE, et al. Differential recognition of canonical NF- κ B dimers by importin α 3. *Nat Commun*. 2022;13:1207.
28. Jimi E, Katagiri T. Critical roles of NF- κ B signaling molecules in bone metabolism revealed by genetic mutations in osteopetrosis. *Int J Mol Sci*. 2022;23:7995.
29. Zhang Q, Lenardo MJ, Baltimore D. 30 years of NF- κ B: a blossoming of relevance to human pathobiology. *Cell*. 2017;168:37-57.
30. Yu H, Lin L, Zhang Z, Zhang H, Hu H. Targeting NF- κ B pathway for the therapy of diseases: mechanism and clinical study. *Signal Transduct Target Ther*. 2020;5:209.
31. Chauhan A, Islam AU, Prakash H, Singh S. Phytochemicals targeting NF- κ B signaling: potential anti-cancer interventions. *J Pharm Anal*. 2022;12:394-405.
32. Bharti AC, Takada Y, Aggarwal BB. Curcumin (diferuloylmethane) inhibits receptor activator of NF- κ B ligand-induced NF- κ B activation in osteoclast precursors and suppresses osteoclastogenesis. *J Immunol*. 2004;172:5940-7.

33. Yang C, Zhu K, Yuan X, Zhang X, Qian Y, Cheng T. Curcumin has immunomodulatory effects on RANKL-stimulated osteoclastogenesis *in vitro* and titanium nanoparticle-induced bone loss *in vivo*. *J Cell Mol Med*. 2020;24:1553-67.
34. Cheemanapalli S, Chinthakunta N, Shaikh NM, Shivaranjani V, Pamuru RR, Chitta SK. Comparative binding studies of curcumin and tangeretin on upstream elements of NF- κ B cascade: a combined molecular docking approach. *Netw Model Anal Health Inform Bioinform*. 2019;8:15.
35. Saeed MEM, Yücer R, Dawood M, Hegazy M-EF, Drif A, Ooko E, et al. *In silico* and *in vitro* screening of 50 curcumin compounds as EGFR and NF- κ B inhibitors. *Int J Mol Sci*. 2022;23:3966.
36. Gauthier-Coles G, Vennitti J, Zhang Z, Comb WC, Xing S, Javed K, et al. Quantitative modelling of amino acid transport and homeostasis in mammalian cells. *Nat Commun*. 2021;12:5282.
37. Qian X, Westensee IN, Fernandes CC, Städler B. Enzyme mimic facilitated artificial cell to mammalian cell signal transfer. *Angew Chem Int Ed Engl*. 2021;60:18704-11.
38. Wan M, Gray-Gaillard EF, Elisseeff JH. Cellular senescence in musculoskeletal homeostasis, diseases, and regeneration. *Bone Res*. 2021;9:41.
39. Zhang L, Wen C. Osteocyte dysfunction in joint homeostasis and osteoarthritis. *Int J Mol Sci*. 2021;22:6522.
40. Llorente I, García-Castañeda N, Valero C, González-Álvaro I, Castañeda S. Osteoporosis in rheumatoid arthritis: dangerous liaisons. *Front Med (Lausanne)*. 2020;7:601618.
41. Epsley S, Tadros S, Farid A, Kargilis D, Mehta S, Rajapakse CS. The effect of inflammation on bone. *Front Physiol*. 2020;11:511799.
42. Chen M, Li Y, Huang X, Gu Y, Li S, Yin P, et al. Skeleton-vasculature chain reaction: a novel insight into the mystery of homeostasis. *Bone Res*. 2021;9:21.
43. Mei L, Li M, Zhang T. MicroRNA miR-874-3p inhibits osteoporosis by targeting leptin (LEP). *Bioengineered*. 2021;12:11756-67.
44. Grässel S, Muschter D. Recent advances in the treatment of osteoarthritis. *F1000Res*. 2020;9:325.

45. Zhen G, Fu Y, Zhang C, Ford NC, Wu X, Wu Q, et al. Mechanisms of bone pain: progress in research from bench to bedside. *Bone Res.* 2022;10:44.
46. Ben Mrid R, Bouchmaa N, Ainani H, El Fatimy R, Malka G, Mazini L. Anti-rheumatoid drugs advancements: new insights into the molecular treatment of rheumatoid arthritis. *Biomed Pharmacother.* 2022;151:113126.
47. Inchingolo AD, Inchingolo AM, Malcangi G, Avantario P, Azzollini D, Buongiorno S, et al. Effects of resveratrol, curcumin and quercetin supplementation on bone metabolism-a systematic review. *Nutrients.* 2022;14:3519.
48. Tabanelli R, Brogi S, Calderone V. Improving curcumin bioavailability: current strategies and future perspectives. *Pharmaceutics* 2021;13:1715.
49. Sabet S, Rashidinejad A, Melton LD, McGillivray DJ. Recent advances to improve curcumin oral bioavailability. *Trends Food Sci Technol.* 2021;110:253-66.
50. Ishtiaq M, Asghar S, Khan IU, Iqbal MS, Khalid SH. Development of the amorphous solid dispersion of curcumin: a rational selection of polymers for enhanced solubility and dissolution. *Crystals.* 2022;12:1606.
51. Mai NNS, Nakai R, Kawano Y, Hanawa T. Enhancing the solubility of curcumin using a solid dispersion system with hydroxypropyl- β -cyclodextrin prepared by grinding, freeze-drying, and common solvent evaporation methods. *Pharmacy (Basel).* 2020;8:203.
52. Sinjari B, Pizzicannella J, D'Aurora M, Zappacosta R, Gatta V, Fontana A, et al. Curcumin/liposome nanotechnology as delivery platform for anti-inflammatory activities via NF κ B/ERK/pERK pathway in human dental pulp treated with 2-HydroxyEthyl MethAcrylate (HEMA). *Front Physiol.* 2019;10:633.
53. Sarkar N, Bose S. Liposome-encapsulated curcumin-loaded 3D printed scaffold for bone tissue engineering. *ACS Appl Mater Interfaces.* 2019;11:17184-92.
54. Wang Q, Liu J, Liu J, Thant Y, Weng W, Wei C, et al. Bisdemethoxycurcumin-conjugated vitamin E TPGS liposomes ameliorate poor bioavailability of free form and evaluation of its analgesic and hypouricemic activity in oxonate-treated rats. *J Nanopart Res.* 2021;23:122.

55. Yeh C-C, Su Y-H, Lin Y-J, Chen P-J, Shi C-S, Chen C-N, et al. Evaluation of the protective effects of curcuminoid (curcumin and bisdemethoxycurcumin)-loaded liposomes against bone turnover in a cell-based model of osteoarthritis. *Drug Des Devel Ther.* 2015;9:2285-300.

56. Kupthammasan N, Wittayarat M, Panichayupakaranant P, Didas N, Wattanachant C, Panyaboriban S. Effects of water-soluble curcuminoid-rich extract in a solid dispersion form (CRE-SD) on the sperm characteristics, longevity and casein kinase II catalytic subunit alpha protein stability in chilled goat semen. *Cryobiology.* 2022;109:30-6.

57. Lateh L, Yuenyongsawad S, Chen H, Panichayupakaranant P. A green method for preparation of curcuminoid-rich *Curcuma longa* extract and evaluation of its anticancer activity. *Pharmacogn Mag.* 2019;15:730.

58. Lateh L, Kaewnopparat N, Panichayupakaranant P, inventors; Pharkphoom Panichayupakaranant, assignee. A method for increasing the water-solubility of curcuminoids and its products, Thailand; *Petty Patent* 2018, 14639.

59. Pengjam Y, Prajantasen T, Tonwong N, Panichayupakaranant P. Downregulation of miR-21 gene expression by CRE-Ter to modulate osteoclastogenesis: *de novo* mechanism. *Biochem Biophys Rep.* 2021;26:101002.

60. Pengjam Y, Panichayupakaranant P, Tanrattanakul V. Curcuminoid (CRE-Ter)/liposome as delivery platform for anti-osteoclastogenesis via NF- κ B/ERK pathways in RANKL-induced RAW 264.7 cells through PLA foams. *Heliyon.* 2021;7:e07823.

61. Agidigbi TS, Kim C. Reactive oxygen species in osteoclast differentiation and possible pharmaceutical targets of ROS-mediated osteoclast diseases. *Int J Mol Sci.* 2019;20:3576.

62. Kumar Rajendran N, George BP, Chandran R, Tynga IM, Houreld N, Abrahamse H. The influence of light on reactive oxygen species and NF- κ B in disease progression. *Antioxidants (Basel).* 2019;8:640.

63. Reis J, Ramos A. In sickness and in health: the oxygen reactive species and the bone. *Front Bioeng Biotechnol.* 2021;9:745911.

64. Gallego-Selles A, Galvan-Alvarez V, Martinez-Canton M, Garcia-Gonzalez E, Morales-Alamo D, Santana A, et al. Fast regulation of the NF- κ B

signalling pathway in human skeletal muscle revealed by high-intensity exercise and ischaemia at exhaustion: role of oxygenation and metabolite accumulation. *Redox Biol.* 2022;55:102398.

65. Quirós-Fallas MI, Vargas-Huertas F, Quesada-Mora S, Azofeifa-Cordero G, Wilhelm-Romero K, Vásquez-Castro F, et al. Polyphenolic HRMS characterization, contents and antioxidant activity of *Curcuma longa* rhizomes from Costa Rica. *Antioxidants (Basel)*. 2022;11:620.

66. Pinzi L, Rastelli G. Molecular docking: shifting paradigms in drug discovery. *Int J Mol Sci.* 2019;20:4331.

67. Yang C, Chen EA, Zhang Y. Protein–ligand docking in the machine-learning era. *Molecules.* 2022;27:4568.

68. Li J, Fu A, Zhang L. An overview of scoring functions used for protein–ligand interactions in molecular docking. *Interdiscip Sci.* 2019;11:320-8.

69. Liu Y, Grimm M, Dai W-T, Hou M-C, Xiao Z-X, Cao Y. CB-Dock: a web server for cavity detection-guided protein–ligand blind docking. *Acta Pharmacol Sin.* 2020;41:138-44.

70. Waddell LA, Lefevre L, Bush SJ, Raper A, Young R, Lisowski ZM, et al. ADGRE1 (EMR1, F4/80) is a rapidly-evolving gene expressed in mammalian monocyte-macrophages. *Front Immunol.* 2018;9:2246.

71. Berman HM, Westbrook J, Feng Z, Gilliland G, Bhat TN, Weissig H, et al. The Protein Data Bank. *Nucleic Acids Res.* 2000;28:235-42.

72. Kim S, Chen J, Cheng T, Gindulyte A, He J, He S, et al. PubChem 2023 update. *Nucleic Acids Res.* 2023;51:D1373-80.

73. Liu Y, Yang X, Gan J, Chen S, Xiao Z-X, Cao Y. CB-Dock2: improved protein–ligand blind docking by integrating cavity detection, docking and homologous template fitting. *Nucleic Acids Res.* 2022;50:W159-64.

74. Hegde M, Girisa S, BharathwajChetty B, Vishwa R, Kunnumakkara AB. Curcumin formulations for better bioavailability: what we learned from clinical trials thus far? *ACS Omega* 2022;8:10713-46.

75. Kunnumakkara AB, Hegde M, Parama D, Girisa S, Kumar A, Daimary UD, et al. Role of turmeric and curcumin in prevention and treatment of

chronic diseases: lessons learned from clinical trials. *ACS Pharmacol Transl Sci.* 2023;6:447-518.

76. Khanizadeh F, Rahmani A, Asadollahi K, Ahmadi MRH. Combination therapy of curcumin and alendronate modulates bone turnover markers and enhances bone mineral density in postmenopausal women with osteoporosis. *Arch Endocrinol Metab.* 2018;62:438-45.

77. Wang C, Wang M, Wang Y, Pan J, Sun C, Zeng Z, et al. Construction and characterization of novel hydrophilic nanospheres loaded with lambda-cyhalothrin via ultrasonic emulsification–solvent evaporation. *Int J Mol Sci.* 2022;23:14063.

78. Danaei M, Dehghankhold M, Ataei S, Hasanzadeh Davarani F, Javanmard R, Dokhani A, et al. Impact of particle size and polydispersity index on the clinical applications of lipidic nanocarrier systems. *Pharmaceutics* 2018;10:57.

79. Wang J, Gong J, Wei Z. Strategies for liposome drug delivery systems to improve tumor treatment efficacy. *A.A.P.S. PharmSciTech.* 2021;23:27.

80. Peram MR, Jalalpure SS, Palkar MB, Diwan PV. Stability studies of pure and mixture form of curcuminoids by reverse phase-HPLC method under various experimental stress conditions. *Food Sci Biotechnol.* 2017;26:591-602.

81. Takechi-Haraya Y, Ohgita T, Demizu Y, Saito H, Izutsu KI, Sakai-Kato K. Current status and challenges of analytical methods for evaluation of size and surface modification of nanoparticle-based drug formulations. *AAPS PharmSciTech.* 2022;23:150.

82. Wahyudiono, He J, Hu X, Machmudah S, Yasuda K, Takami S, et al. Curcumin-loaded liposome preparation in ultrasound environment under pressurized carbon dioxide. *Foods.* 2022;11:1469.

83. Csicsák D, Szolláth R, Kádár S, Ambrus R, Bartos C, Balogh E, et al. The effect of the particle size reduction on the biorelevant solubility and dissolution of poorly soluble drugs with different acid-base character. *Pharmaceutics* 2023;15:278.

84. Lee M-K. Liposomes for enhanced bioavailability of water-insoluble drugs: *in vivo* evidence and recent approaches. *Pharmaceutics* 2020;12:264.

85. Paradkar A, Ambike AA, Jadhav BK, Mahadik KR. Characterization of curcumin–PVP solid dispersion obtained by spray drying. *Int. J. Pharm.* 2004;271:281-6.
86. Chhouk K, Diono W, Kanda H, Goto M. Micronization for enhancement of curcumin dissolution via electrospraying technique. *ChemEngineering* 2018;2:60.
87. Machmudah S, Winardi S, Wahyudiono, Kanda H, Goto M. Formation of fine particles from curcumin/PVP by the supercritical antisolvent process with a coaxial nozzle. *ACS Omega* 2020;5:6705-14.
88. Laouini A, Charcosset C, Fessi H, Holdich RG, Vladisavljević GT. Preparation of liposomes: a novel application of microengineered membranes - investigation of the process parameters and application to the encapsulation of vitamin E. *RSC Adv.* 2013;3:4985-94.
89. Ileri Ercan N. Understanding interactions of curcumin with lipid bilayers: a coarse-grained molecular dynamics study. *J Chem Inf Model.* 2019;59:4413-26.
90. Trott O, Olson AJ. AutoDock Vina: improving the speed and accuracy of docking with a new scoring function, efficient optimization, and multithreading. *J Comput Chem.* 2010;31:455-61.
91. Zhao J, Cao Y, Zhang L. Exploring the computational methods for protein-ligand binding site prediction. *Comput Struct Biotechnol J.* 2020;18:417-26.
92. Tian W, Chen C, Lei X, Zhao J, Liang J. CASTp 3.0: computed atlas of surface topography of proteins. *Nucleic Acids Res.* 2018;46:W363-7.
93. Riedlinger T, Liefke R, Meier-Soelch J, Jurida L, Nist A, Stiewe T, et al. NF- κ B p65 dimerization and DNA-binding is important for inflammatory gene expression. *FASEB J.* 2019;33:4188-202.

APPENDIX

Appendix A: The triplicate data of microscopic images, gel images, and blot images

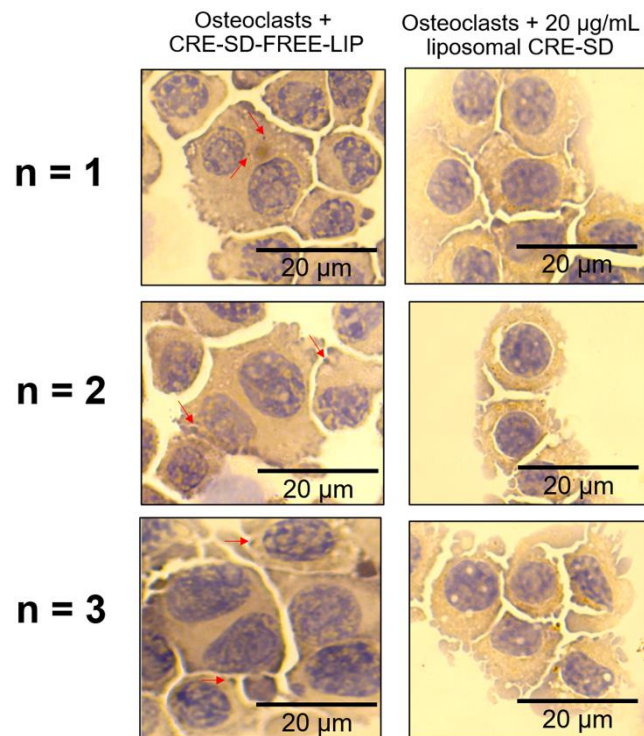


Figure A1 Triplicate microscopy images of 20 ng/mL RANKL-stimulated RAW 264.7 cells (osteoclasts) after TRAP staining following treatment with CRE-SD-free POPC liposomes (CRE-SD-FREE-LIP) and 20 μ g/mL liposomal CRE-SD

The arrows indicate stained granules.

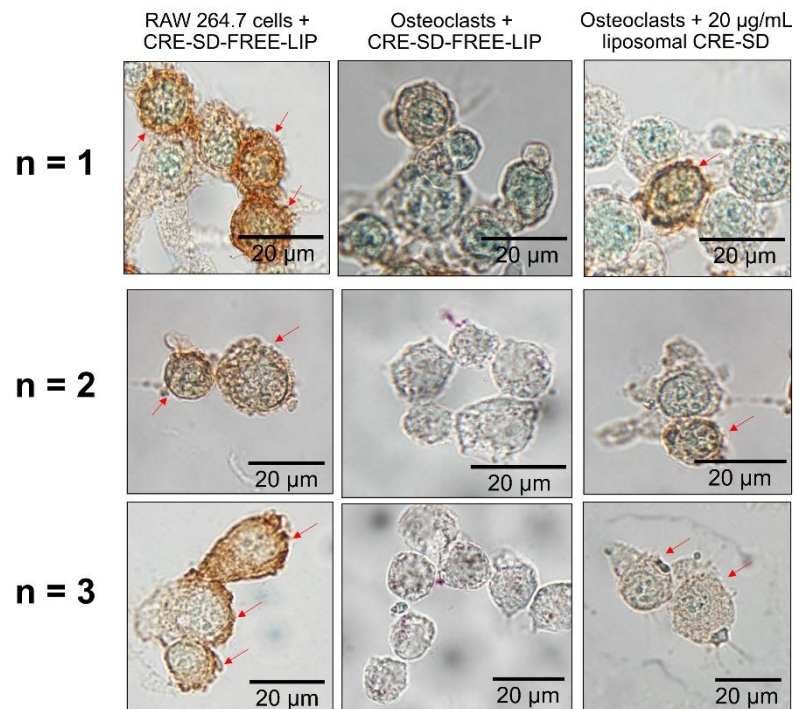


Figure A2 Triplicate microscopy images of 20 ng/mL RANKL-stimulated RAW 264.7 cells (osteoclasts) after the immunocytochemistry analysis of F4/80

RANKL-unstimulated RAW 264.7 cells treated with CRE-SD-FREE-LIP and 20 ng/mL RANKL-stimulated RAW 264.7 cells treated with CRE-SD-FREE-LIP and 20 µg/mL liposomal CRE-SD were examined. The arrows indicate F4/80-positively stained cells.

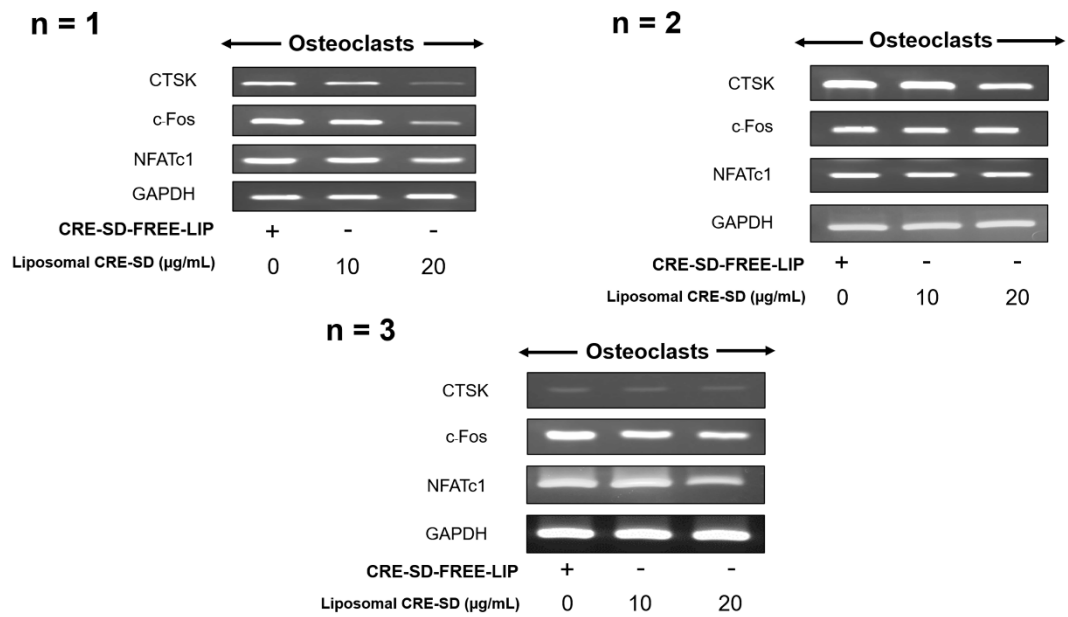


Figure A3 Triplicate images of gels analyzing 20 ng/mL RANKL-stimulated RAW 264.7 cells (osteoclasts) following RT-PCR analysis of CTSK, c-Fos, and NFATc1

The 20 ng/mL RANKL-stimulated RAW 264.7 cells were treated with CRE-SD-FREE-LIP and liposomal CRE-SD (10 and 20 µg/mL).

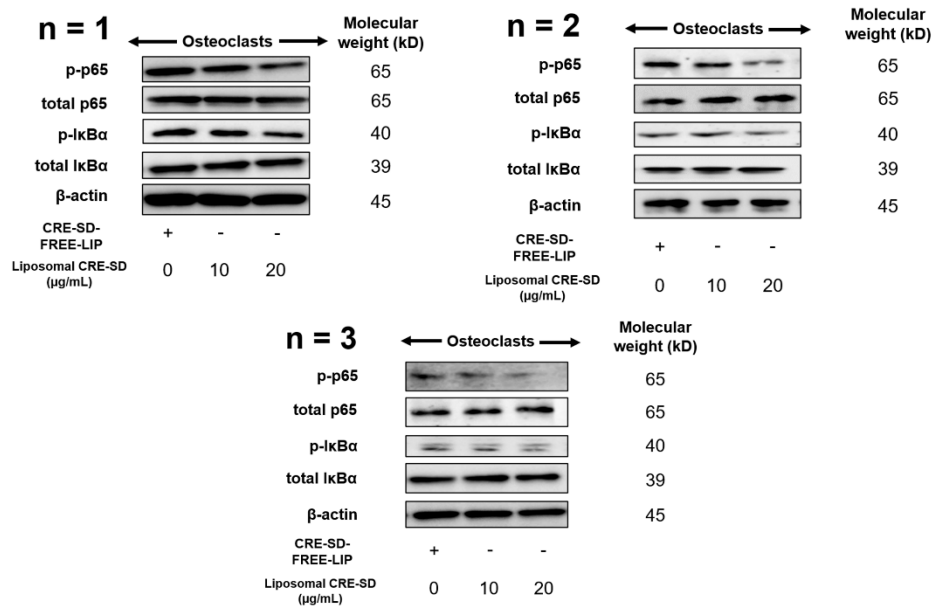


Figure A4 Triplicate images of blots analyzing 20 ng/mL RANKL-stimulated RAW 264.7 cells (osteoclasts) following the detection of the phosphorylation of p65 and IκBα

The 20 ng/mL RANKL-stimulated RAW 264.7 cells were treated with CRE-SD-FREE-LIP and liposomal CRE-SD (10 and 20 μg/mL).

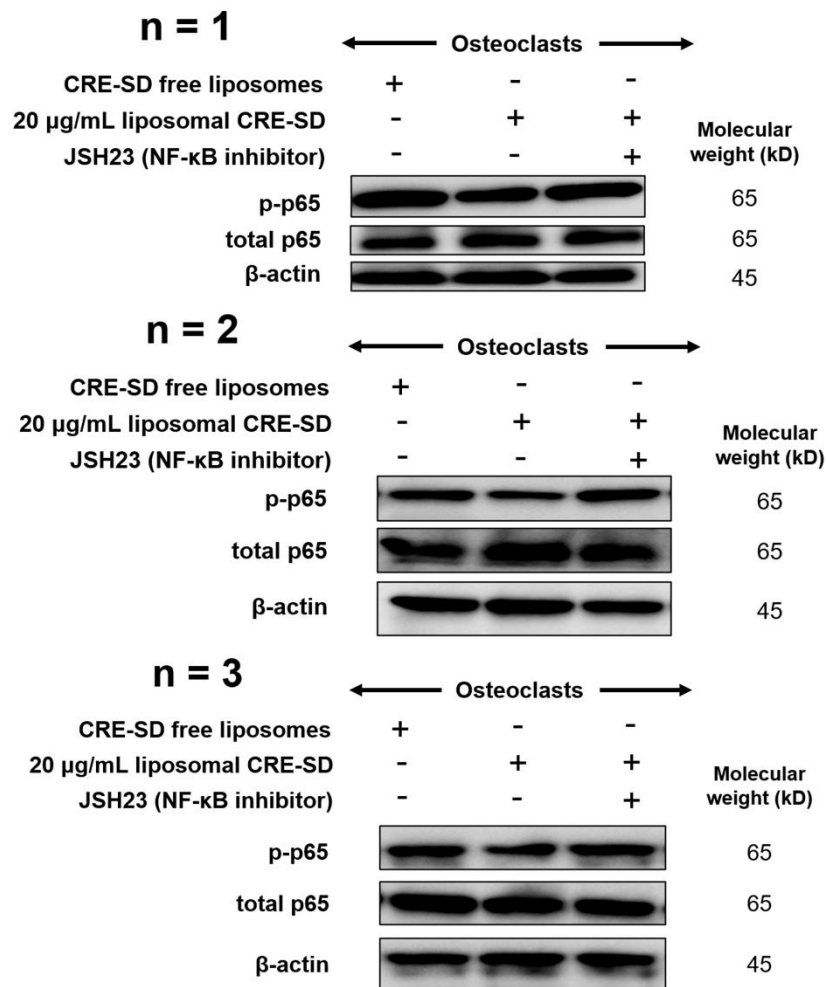


Figure A5 Triplicate images of blots of 20 ng/mL RANKL-stimulated RAW 264.7 cells (osteoclasts) for detecting the nuclear translocation and transcriptional activity of p-p65

VITAE

Name Mr.Sompot Jantarawong

Student ID 6410220042

Educational Attainment

Degree	Name of Institution	Year of Graduation
Bachelor of Science in Medical Technology (First Class Honors)	Prince of Songkla University	2021

Scholarship Awards during Enrolment

Faculty of Medical Technology Research Fund, Prince of Songkla University, Thailand
Thesis Research Grant in the Fiscal Year 2022, Graduate School, Prince of Songkla University, Thailand

Work – Position and Address

2021-2023

Research assistant, Faculty of Medical Technology, Prince of Songkla University, Songkhla 90110, Thailand

List of Publication and Proceedings

Publication

Jantarawong S, Swangphon P, Lauterbach N, Panichayupakaranant P, Pengjam Y. Modified curcuminoid-rich extract liposomal CRE-SD inhibits osteoclastogenesis via the canonical NF- κ B signaling pathway. *Pharmaceutics* 2023; 15:2248.

(This article belongs to the Special Issue Advanced Liposomes for Drug Delivery of the journal *Pharmaceutics*)

VITAE (continued)**Publication (continued)****Awaiting reviewer assignment (R1: first revision)**

Inchai J, Numit A, Jantarawong S, Chunta S, Swangphon P, Panichayupakaranant P, Pengjam Y. Curcuminoid (CRE-Bin) induces osteogenic initiation and inhibits osteoclast differentiation through Wnt/ β -catenin and NF- κ B/Akt Signaling Pathways. Chinese Herb. Med. ? (Manuscript ID: CHM-2022-0125.R1)

Oral presentation during the thesis

Jantarawong S, Prajantasen T, Tonwong N, Panichayupakaranant P, Pengjam Y. Downregulation of miR-21 gene expression by CRE-Ter to modulate osteoclastogenesis: *de novo* mechanism. Paper presented at: The 36th International Annual Meeting in Pharmaceutical Sciences (IAMPS36) and Herbal and Traditional Medicine 2021 (HTM 2021); 2021 May 28; Online Conference.

Poster presentation during the thesis

Jantarawong S, Yamaguchi Y, Hasegawa K, Sani A, Khimmaktong W, Panichayupakaranant P, Pengjam Y. Studying the effects of Asian herbal medicines for the treatment of sarcopenia patients. Poster session presented at: The 100th Anniversary Meeting of the Physiological Society of Japan; 2023 March 16; Kyoto, Japan.